Electrical stimulation at nanoscale topography boosts neural stem cell neurogenesis through the enhancement of autophagy signaling

Article *in* Biomaterials · January 2021

DOI: 10.1016/j.biomaterials.2020.120585

CITATIONS
16

READS
153

16 authors, including:

He Liumin
Sun Yat-Sen University
69 PUBLICATIONS **1,764** CITATIONS
SEE PROFILE

Sun Zhongqing
The University of Hong Kong
6 PUBLICATIONS **99** CITATIONS
SEE PROFILE

Jianshuang Li
Jinan University (Guangzhou, China)
25 PUBLICATIONS **654** CITATIONS
SEE PROFILE

Kwok-Fai So
The University of Hong Kong
566 PUBLICATIONS **19,472** CITATIONS
SEE PROFILE

Biomaterials 268 (2021) 120585

Contents lists available at ScienceDirect

Biomaterials

journal homepage: www.elsevier.com/locate/biomaterials

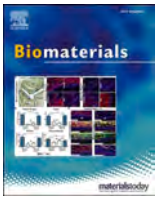

Electrical stimulation at nanoscale topography boosts neural stem cell neurogenesis through the enhancement of autophagy signaling

Liumin He [a,f,*,1], Zhongqing Sun [b,1], Jianshuang Li [c,d,1], Rong Zhu [b,e], Ben Niu [b], Ka Long Tam [g], Qiao Xiao [e], Jun Li [e], Wenjun Wang [d], Chi Ying Tsui [g], Vincent Wing Hong Lee [b], Kwok-Fai So [b,e,i], Ying Xu [e], Seeram Ramakrishna [e,h], Qinghua Zhou [c,d,***], Kin Chiu [b,i,**]

[a] Department of Spine Surgery, The 3rd Affiliated Hospital, Sun Yat-Sen University, Guangzhou, 510630, PR China
[b] Department of Ophthalmology, Li Ka Shing Faculty of Medicine, The University of Hong Kong, Hong Kong SAR, PR China
[c] Zhuhai Institute of Translational Medicine Zhuhai People's Hospital Affiliated with Jinan University, Jinan University, Zhuhai, 519000, Guangdong, PR China
[d] The First Affiliated Hospital, The Biomedical Translational Research Institute, Faculty of Medical Science, Jinan University, Guangzhou, 510632, Guangdong, PR China
[e] MOE Joint International Research Laboratory of CNS Regeneration, Guangdong-Hong Kong-Macau Institute of CNS Regeneration (GHMICR), Jinan University, Guangzhou, 510632, PR China
[f] College of Life Science and Technology, Jinan University, Guangzhou, 510632, Guangdong, PR China
[g] Department of Electronic and Computer Engineering, The Hong Kong University of Science and Technology, Hong Kong SAR, PR China
[h] Department of Mechanical Engineering, Faculty of Engineering, National University of Singapore, Singapore, 117576, Singapore
[i] State Key Laboratory of Brain and Cognitive Sciences, The University of Hong Kong, Hong Kong SAR, PR China

ARTICLE INFO

Keywords:
Neural stem cell
Electrical stimulation
Differentiation
Carbon nanotubes
Autophagy

ABSTRACT

Neural stem cells (NSCs) transplantation at the injury site of central nerve system (CNS) makes it possible for neuroregeneration. Long-term cell survival and low proliferation, differentiation, and migration rates of NSCs-graft have been the most challenging aspect on NSCs application. New multichannel electrical stimulation (ES) device was designed to enhance neural stem cells (NSCs) differentiation into mature neurons. Compared to controls, ES at nanoscale topography enhanced the expression of mature neuronal marker, growth of the neurites, concentration of BDNF and electrophysiological activity. RNA sequencing analysis validated that ES promoted NSC-derived neuronal differentiation through enhancing autophagy signaling. Emerging evidences showed that insufficient or excessive autophagy contributes to neurite degeneration. Excessive ES current were able to enhance neuronal autophagy, the neuronal cells showed poor viability, reduced neurite outgrowth and electrophysiological activity. Well-controlled autophagy not only protects against neurodegeneration, but also regulates neurogenesis. Current NSC treatment protocol efficiently enhanced NSC differentiation, maturation and survival through combination of proper ES condition followed by balance of autophagy level in the cell culture system. The successful rate of such protreated NSC at injured CNS site should be significantly improved after transplantation.

1. Introduction

Degenerative diseases and traumatic injuries to the central nerve system (CNS) cause neuron death with consequent destruction of neural circuitry, leading to the loss of neuronal function. As multipotent stem cells present in the CNS, neural stem cells (NSCs) have the ability to differentiate into a vast array of more specialised CNS cells such as neurons, astrocytes and oligodendrocytes [1]. Neurons derived from grafted NSCs have been experimentally documented to extend large numbers of axons from lesion sites to form synapses with host axons that

* Corresponding author. Department of Spine Surgery, The 3rd Affiliated Hospital, Sun Yat-Sen University, Guangzhou 510630, PR China.
** Corresponding author. Department of Ophthalmology, Li Ka Shing Faculty of Medicine, The University of Hong Kong, Room 409, Hong Kong Jockey Club Building for Interdisciplinary Research, 5 Sassoon Road, Pokfulam, Hong Kong SAR, PR China.
*** Corresponding author. The First Affiliated Hospital, The Biomedical Translational Research Institute, Faculty of Medical Science, Jinan University, Guangzhou, 510632, Guangdong, PR China.
E-mail addresses: helm9@mail.sysu.edu.cn (L. He), gene@email.jnu.edu.cn (Q. Zhou), datwai@hku.hk (K. Chiu).
[1] These authors contributed equally to this work.

https://doi.org/10.1016/j.biomaterials.2020.120585
Received 4 September 2020; Received in revised form 13 November 2020; Accepted 25 November 2020
Available online 2 December 2020
0142-9612/

can serve as neural relays across the lesion site to support functional improvement [2–4]. Exogenous NSCs transplantation exerted positive therapeutic effects in various CNS diseases, including ischemic stroke, traumatic brain injury and neurodegenerative disease [1,5,6]. However, current NSC-based approaches are blocked by a number of hurdles, including NSC migration involving, for example, proliferation, maturation, and integration and, although pretreatment of NSCs through exposure to small molecules and/or cytokines prior to transplantation has proven effective in promoting performance and enhancing functional recovery in pre-clinical in vivo settings [7,8], optimized and feasible protocols are still required to ensure the efficacy of NSC neurogenesis.

Dynamic electrical signals are present in the extracellular spaces between neural cells, while steady electrical signals exist across contiguous cytoplasmic regions within cells [9]. The electrical stimulation (ES) of exogenous electrical signals therefore enables the successful control of NSC fate in terms of proliferation [10], migration [11,12], differentiation [11], etc. Moreover, ES enhanced spontaneous regeneration and significantly increase replenish progenitor cells that expressed nestin and other markers after spinal cord injury of adult rats [13]. ES on NSC transplantation significantly boosts nerve regeneration after peripheral nerve trauma [14]. Electrically preconditioned human neural progenitor cells (hNPCs) on conductive polymer scaffold enhanced long-term function recovery in a stroke model [15]. In the APP/PS1 transgenic mice, Li and his coworker observed that ES promoted neurogenesis, increased the expression of BDNF and improved neurobehaviors [16].

A recent study found that electrical muscle stimulation following nerve injury increased the number of autophagosomes and the expression of LC3-IIautophagy markers while decreasing the level of autophagy substrate protein P62 in distal nerve segments [17]. ES was also found to increase the protein concentrations of Beclin-1 and the LC3 II/I ratio in a patient's diaphragm during cardio-thoracic surgery [18]. These studies represented attempts at linking electrical phenomena to autophagy, which has become a generally accepted protective mechanism for maintaining cellular homeostasis by recycling intracellular components. A growing body of evidence suggests that autophagy signalling is involved in the machinery related to the biological behaviours of NSCs [19–21] and that autophagy can provide sufficient energy and metabolic substrates for NSC differentiation through the reuse of intracellular components [22,23]. ES involves the delivery of a low-level electrical current and/or electrical field to produce an exogenous stimulus pressure to cells and, although autophagy is thought to play a critical role in the manipulation of NSC physiological reaction through ES, to date there has been limited research to verify the connection.

With the goal of establishing and exploring the connection between ES and enhanced autophagy, in this study NSCs were cultured on an electrically conductive substrate fabricated through the layer-by-layer assembly of negatively charged carbon nanotubes (CNTs) and positively charged polymers [24–26] and a multi-chambered ES device was specially designed to provide stable ES with manipulable parameters. This work demonstrated that the previously uncharacterised role of autophagy is an important acting pathway for the promotion of neuronal differentiation and NSC maturation via ES. The findings of our pioneering study shed more light on the molecular mechanisms for potentially enhancing NSC neurogenesis through the application of exogenous electric cues mediated by nano-scaled biomaterials and provide profound insights for future applications of ES in the pre-conditioning of NSCs prior to transplantation for neural regeneration.

2. Results

2.1. Neurite outgrowth of NSC-derived neurons under ES

The experiments in this study were carried out using a unique multi-chambered ES setup in which a high-impedance source supplied tunable current through parallel-plate carbon electrodes anchored to the lids of a cell culture plate (Fig. 1A). The electrodes were fabricated from inert carbon, which is resistant to severe decomposition during electrolysis. All elements of the setup were either handmade or manufactured via fine machining [27]. The assembled carbon electrodes were connected to CNT-multilayered films placed at the bottoms of the chambers, enabling the independent application of ES signals with various parameters (e.g., stimulation current amplitude, pulsing frequency and stimulation duration) to each chamber through a data acquisition device. Using this layout, it was possible, unlike in previous studies, to provide multiple ES platforms for cell investigation at a large scale.

ES signals of differing current and duration were administrated to NSCs cultured in a differentiation medium on the CNT-multilayered films for 7 d each (Fig. 1B), with ES administrated on days three, four, and five post-NSC seeding in the CMP-ES group. As shown in Fig. 1, the NSCs were able to differentiate into neurons with long neurites after 7 d under different ES conditions, as revealed by the presence of the neuron-specific cytoskeletal marker β III tubulin (TUJ1) and microtubule-associated protein 2 (MAP2). The application of ES significantly promoted neurite outgrowth relative to the control group (CMP), with the degree of promotion showing a dependence on both current and duration. At a current of 1 mA, neurite length continually increased with stimulation time from 0 to 2 h but slowed down at 3 h, with no significant differences from the length measured at 2 h. Similarly, at a current of 2 mA, neurite length was found to increase in a sustained manner with stimulation time within a 2 h duration but subsequently decreased with stimulation up to 3 h. These results indicated that moderate-intensity ES was beneficial to neurite outgrowth and that the ES parameters should be screened prior to application. Neurons create connections through extensions of their cellular body called neurites, the outgrowth of which plays a critical role in the construction of neuronal circuitry. As the NSC-derived neurons produced the longest neurites following ES at 20 Hz for 2 h per day, these ES parameters were utilized in the succeeding studies.

To evaluate effect of ES and nano-scaled substrate on the morphology of NSC-derived neurons, neuron-specific cytoskeletal marker β III tubulin staining was performed and data were investigated using Neurolucida software (Fig. 2A). Results demonstrated that the average neurite length (Fig. 2B) and total length (Fig. 2C) per neuron were lower on CMP group (64.063 ± 28.984 μm, 543.288 ± 220.102 μm) than on those on PDL-coated substrate (133.257 ± 83.276 μm, 614.529 ± 255.448 μm). Following administration of ES, both indexes of neurite length were almost doubled, and the total neurite length per cell of CMP-ES group was even significantly higher than PDL group. Besides, a similar trend was also observed in the average branch number of per cell (Fig. 2D). The average branch number of CMP-ES group (20.7 ± 8.16) was almost doubled than that of CMP group (10.9 ± 6.28), which was even higher than PDL group (15.4 ± 9.34). Compared with CMP group, ES significantly increase the cell number on the day 7. The cell number in PDL was also higher than that in CMP group (SFig. 1).

As neurite outgrowth was primarily dominated by the interactions between the neurites and substrates, growth cone filopodia played an important role in determining the synaptic connection of neurites with target neurons [28]. These were further evaluated through the GAP-43 and F-actin immunochemistry staining together with β III tubulin labelling on the NSC-derived neurons to investigate the interactions between the neurites and substrates. As shown in Fig. 2E, more F-actin immunoreactive filopodia and lamellipodia were observed on the NSC-derived neurons cultured on the CMP substrates than those on the PDL substrate, and it appeared even more after electrical stimulation. Further analysis was utilized to verify that, the puncta number per 10 μm of CMP group (3.79 ± 1.27) were significantly higher than PDL group (2.46 ± 1.05) (Fig. 2F). The puncta number and puncta length per 10 μm of CMP-ES group (3.91 ± 0.84, 6.10 ± 2.45) were almost double than the PDL group (Fig. 2F and G). Meanwhile , the average relative puncta density of CMP-ES group was significantly higher than that of CMP group (Fig. 2H). GAP-43 is a nervous-tissue-specific protein and is

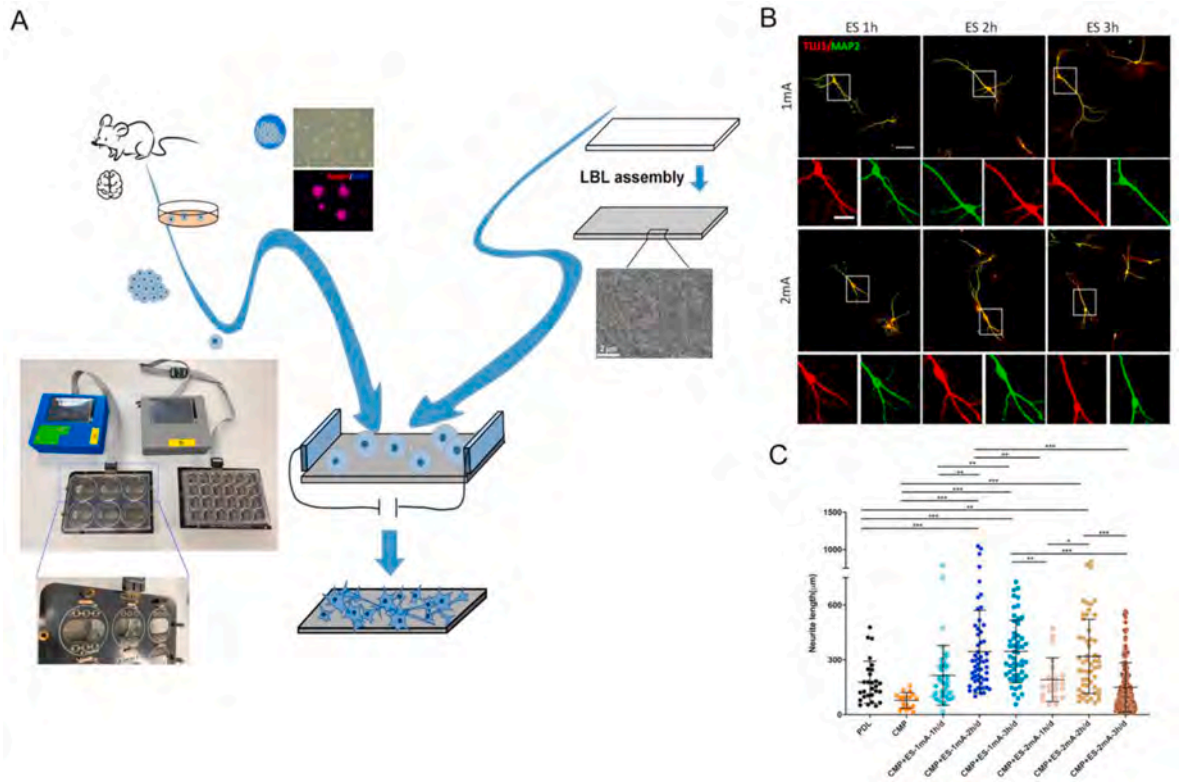

Fig. 1. Differentiation of NSC cultured on the CNT-multilayered substrates under various ES conditions. (a) Schematic diagram of experimental multi-channel ES setup in this study. (b) Representative immunofluorescence staining of NSC-derived neurons cultured on the CNT-multilayered substrates with ES signals of different intensity applied for 7 d, (Scale bars = 100 μm) and separate channels with higher magnificantion (Scale bars = 50 μm). (c) Neurite lengths measured and quantitatively analysed using ImageJ software. $^{*}p < 0.05$, $^{**}p < 0.01$, $^{***}p < 0.001$.

expressed in neurites, lamellipodia, and filopodia, where it associates tightly with the cortical membrane skeleton. Compared with PDL and CMP group, abundant immunoreactive lamellipodia and filopodia along the long neurites and fan-like filopodia on the growth cone were significantly observed on the CMP-ES group (Fig. 2I), which inferred that ES could conduce to construct the synaptic connections and guide extension of axonal projection to specific targets. Besides, the BDNF content in the supernatant of the cell culture medium increased from 7 day to 14 day, after 14days culture, the CMP-ES group (25.517 ± 7.626 pg/ml) shown the highest BDNF concentration, which was significantly higher than the CMP group (14.649 ± 3.637 pg/ml), and almost doubled than PDL group (11.635 ± 2.302 pg/ml) (Fig. 2J). BDNF is a secretory growth factor that supports the phenotypic maintenance of mature neurons and promotes synaptogenesis [29]. Thus, the promotion of BDNF secretion by the application of ES exerted a pro-survival, pro--maturing effect on the neurons. Collectively, these results suggested that the CNT-multilayered films provided a permissive microenvironment for neurite outgrowth and that the ES further enhanced the affinity between the NSC-derived neurons and the CNT-based substrate, enabling the further modulation of growth cone motility and promoting neurite outgrowth [30].

2.2. ES-promoted NSC differentiation into mature neurons

To better understand the effects of ES on the neuronal differentiation and maturation process of NSCs, Doublecortin (DCX), TUJ1, MAP2 and NeuN were used to label NSC-derived neurons after cultured in a differentiation medium for 7 and 14 d. As shown in Fig. 3, after 7 days of differentiation and culture (Fig. 3A), the expression of DCX and TUJ1 in each group was obvious, while MAP2 and NeuN were not completely expressed. After the NSCs were cultured for 14 days, the expression of DCX was significantly reduced, and TUJ1, MAP2, and NeuN were all in a high expression state (Fig. 3B). Measurements of average fluorescence intensity revealed that, after 14 d, the DCX expression of the CMP-ES group (0.051 ± 0.008) was significantly lower than that in the CMP group (0.082 ± 0.019), while the NeuN expression in the CMP-ES group (0.091 ± 0.006), was significantly increased relative to that of the CMP group (0.076 ± 0.009) (Fig. 3C and D). A similar trend appeared in the mRNA expression test on day 7 (Fig. 3E), but the mRNA expression of DCX and NeuN on day 14 shown different message (Fig. 3F), which inferred that ES at CNT-multilayered films could accelerate the differentiation process of NSCs to neurons, and appear mature neuron markers earlier than the CMP group.

2.3. Effects of ES on the electrophysiological features of NSC-derived neurons

The electrophysiological characteristics of NSC-derived neurons were investigated using the patch clamp technique, with sodium and potassium currents recorded in the neurons of all the three groups after 7 and 14 d of differentiation cultivation (SFig. 2). The peak amplitude of the recorded sodium-potassium currents was higher at day 14 than at day seven, indicating a gradual increase in the maturation of the NSC-derived neurons. However, following 7 d of differentiation culturing of the NSC, very few action potential (AP) spikes were detected in the neurons of any of the three groups. Although small numbers of APs were released after 10 d, these were unstable (SFig. 2C). Mature AP spikes were occurring by 14 d, as confirmed by the broaching of the 0-mV membrane potential, along with the presence of fast depolarisation and repolarisation, which could be blocked by the sodium channel blocker tetrodotoxin (TTX) (Fig. 4A). The peak AP amplitude of the CMP group was lower (47.99 ± 6.08 mV) than that of the PDL group and had an unstable frequency (25.60 ± 2.26 Hz), while the peak amplitude and frequency of the CMP-ES group was higher and more stable (73.20 ±

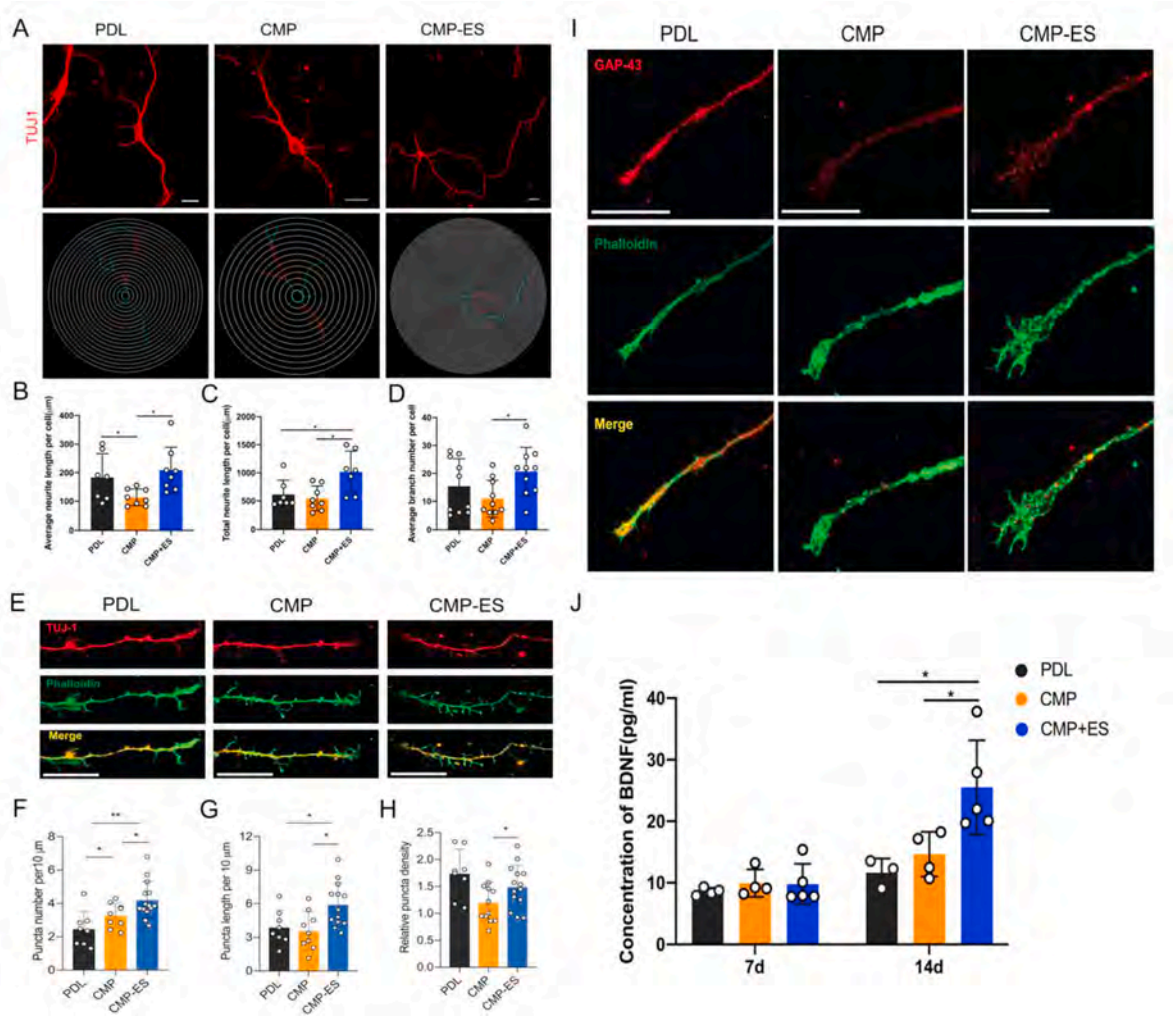

Fig. 2. ES promoted the neurite outgrowth and spine puncta density of NSC-derived neurons. (a) Representative images of neuron-specific cytoskeletal marker β-III-tubulin (anti-TUJ1) staining of neurons derived from NSCs cultured on PDL, CMP, and CMP-ES substrates for 7 d. The neuron cytoskeleton is reconstructed using Neurolucida software. The statistical results reveal that the average neurite length (b) and total neurite length per neuron (c) on the CMP were lower than those on PDL-coating substrate. Following electrical stimulation (ES), both indexes were significantly increased relative to both the PDL and CMP groups; the average branch number in the ES group was also higher than in the other two groups (d). Scale bars = 20 μm (e) Representative images of spine puncta stained with β-III-tubulin (anti-TUJ1) and phalloidin on PDL, CMP, and CMP-ES substrates for 7 d. The spine puncta density is measured using ImageJ software. The statistical results reveal that the puncta number per 10 μm (f) and puncta length per 10 μm (g) on the CMP ES were longer than those on CMP and PDL-coating substrate. The relative puncta density in the ES group was also higher than in the other two groups (h). (i) Compared with the short filopodia and lamellipodia found on the PDL-coating substrate, neurites on the CMP and CMP-ES had abundant filopodia and lamellipodia, along with longer neurites and fan-like filopodia on the growth cone (arrows). Scale bars = 10 μm.(j)BDNF content in the supernatant of each group at different cultivation times by ELISA. There is no significant difference of BDNF secretion between PDL, CMP and CMP-ES on the day 7. While the release of BDNF in the ES group was also higher than in the PDL and CMP group, n = 5. *p < 0.05 and **p < 0.01.

6.20 mV; 39.58 ± 2.14 Hz) (Fig. 4B and C). The percentage of NSC-derived neurons in the CMP-ES group exhibiting repetitive mature APs (53%) was also larger than in the other two groups (PDL, 42%; CMP, 30%) (Fig. 4D). Following TTX blockading, the AP peak amplitude rapidly decreased to 35.46% of the pre-blockade value (Fig. 4E). Messages transmitted down an axon are essentially electrical/chemical events, with APs used to set off the chains of events that 'fire' the neuron; as such, APs play a central role in neuronal communication by enabling the propagation of signals at synapses. Accordingly, these AP-related results indicate that the electrophysiological features of NSC-derived neurons were enhanced by ES, which therefore potentially promoted functional neuronal maturation.

Spontaneous synaptic currents were recorded in the NSC-derived neurons after 14 d (Fig. 4F), at which point positive staining of post-synaptic protein-95 (PSD-95) was observed in the NSC-derived neurons of all three groups, confirming the presence of information processing between the neurons (SFig. 3). In a manner similar to their promotion of APs, ES increased both the frequency and peak amplitude of spontaneous synaptic currents (Fig. 4G and H). We also found that the spontaneous synaptic currents of the CMP group were concentrated primarily in the small-amplitude region, while spontaneous synaptic events in the higher-amplitude regions were recorded in the NSC-derived neurons of the CMP-ES group (Fig. 4I), suggesting that these neurons showed higher maturity and probably formed synaptic connections with other neurons [31,32].

Calcium ions generate versatile intracellular signals that can elicit responses such as altered gene expression and neurotransmitter release from synaptic vesicles, controlling the key functions of neurons [33]. Calcium imaging was utilized to monitor intracellular calcium in the NSC-derived neurons cultured under ES in real time. Following 14 d of differentiation cultivation, cells were labelled with a Ca^{2+}-sensitive indicator, Fluo-2 AM. An increase in the fluorescence of intracellularly labelled Ca^{2+} was triggered immediately upon exposure to ES (20 Hz, 1 mA) with a levelling-off in cell fluorescence occurring after turning the

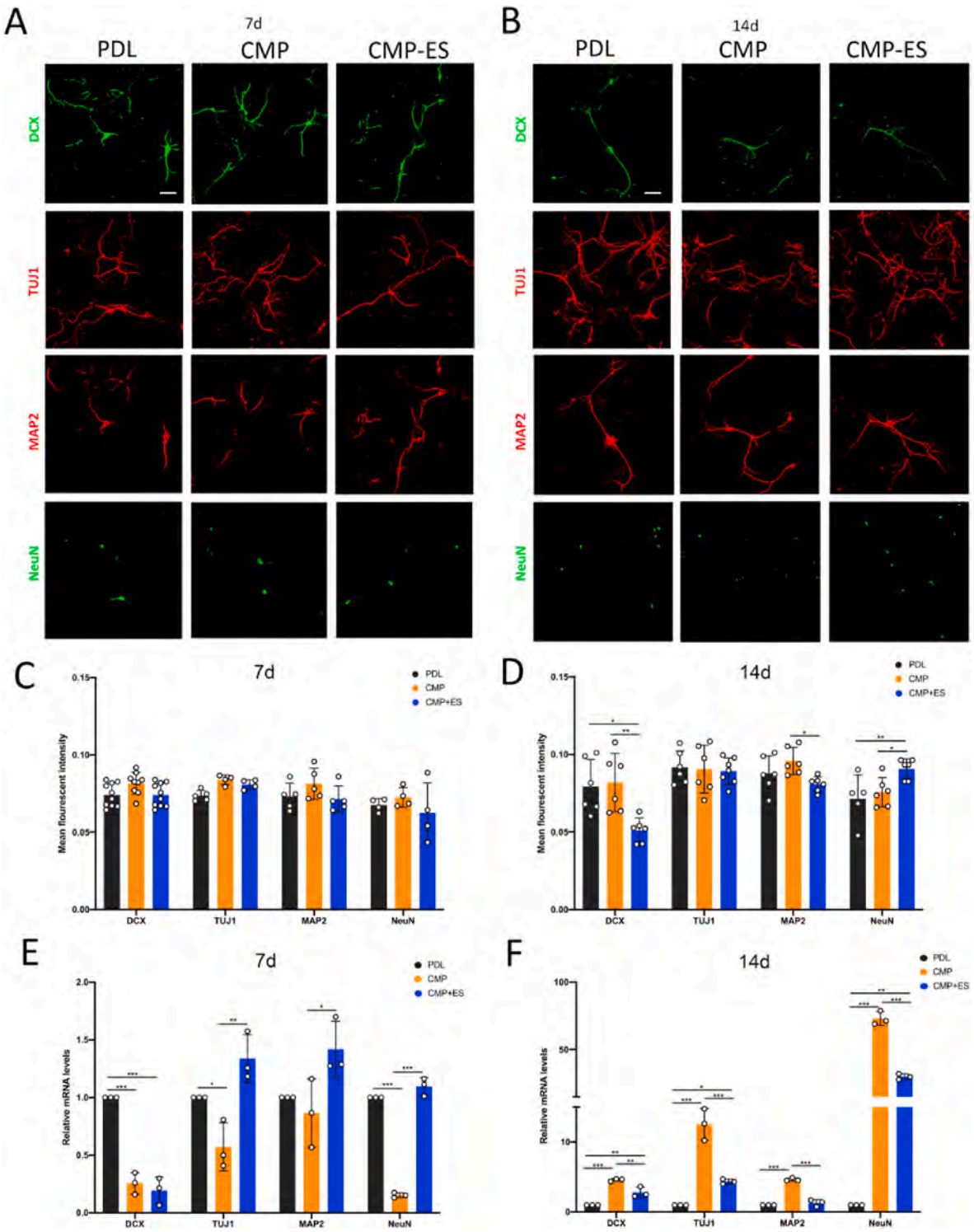

Fig. 3. ES-promoted NSC differentiation into mature neurons. (a, b) Immunochemical DCX and NeuN staining of NSC-derived neurons at different cultivation times. (c, d) Average fluorescence of DCX and NeuN markers. The expression of DCX and NeuN in cells decreased and increased gradually with culture time, respectively. (e, f) The mRNA expression of DCX and NeuN were increased significantly at 7 d; at 14 d, the expression was less pronounced in the CMP-ES group than in the CMP group. n = 6, *p < 0.05 and **p < 0.01. Scale bar = 20 μm n = 6 *p < 0.05 and **p < 0.01.

ES off (see arrows in SFig. 4A). Observation of the fluorescence over stimulation time revealed that the peaking fluorescence under ES was double that prior to ES and decreased to the initial level after ES (SFig.4B, C, and SVideo. 1), indicating that cell signals besides spontaneous firing were indeed initiated by the ES, in close agreement with the results of previous work [34]. In our previous study, we documented the promotion by CNT-multilayered nanomaterials of the electrophysiological maturity of NSC-derived neurons in the absence of chemical agents typically required for neurogenesis, probably as a result of the favouring of electrical shortcuts between the proximal and distal compartments of the neuron [35,36]. In the current study, the administration of exogenous ES exerted little influence on the NSC-derived neurons cultured on PDL coating, which is not electrically conductive. These results, therefore, indicate that exogenous ES-initiated current

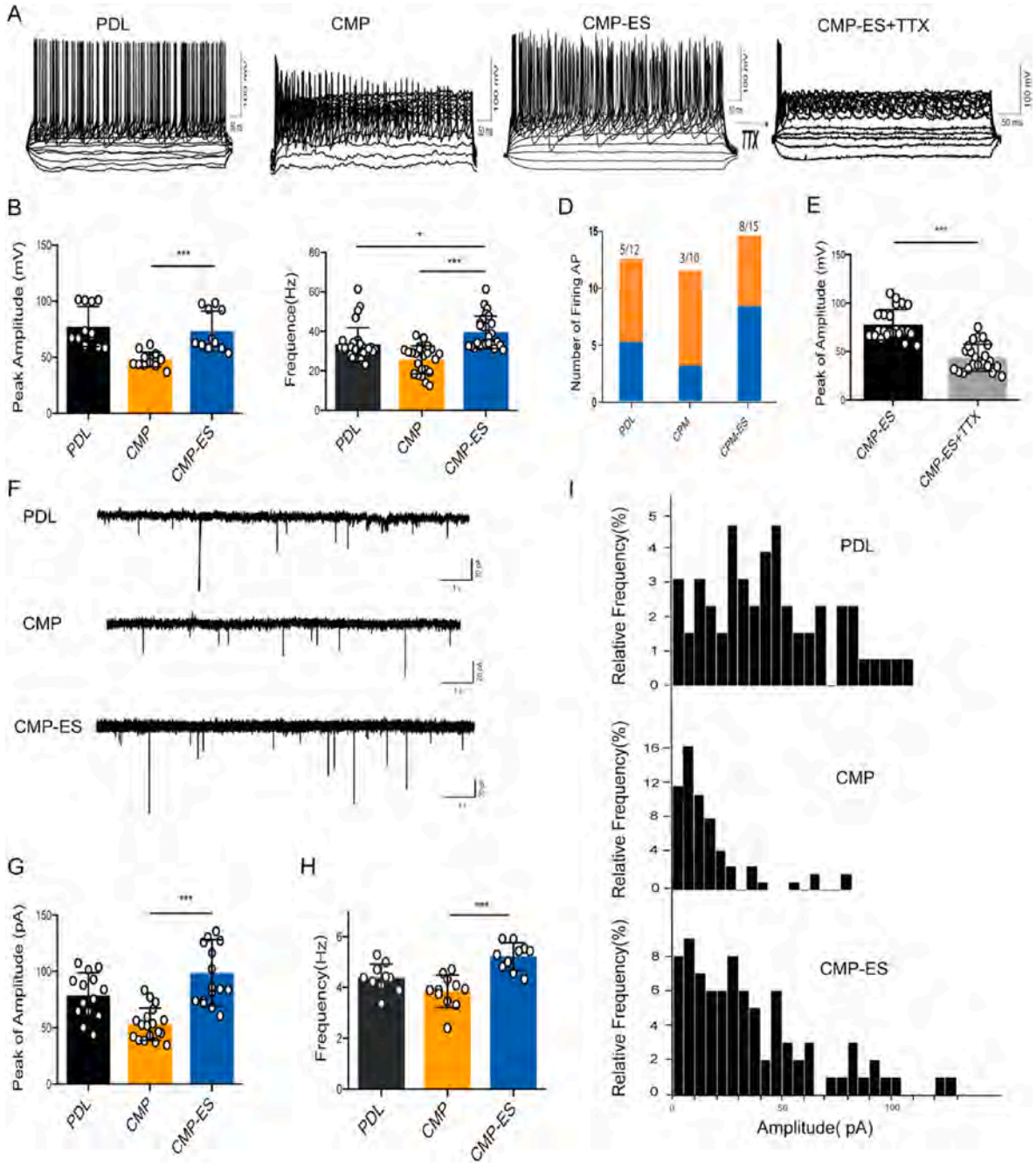

Fig. 4. Electrical characteristics of NSC-derived neurons. (a) Action potential (AP) firings of NSC-derived neurons recorded via current-clamp after culturing NSCs in differentiation media for 14 d. Scale bars: 100 mV and 50 ms (left of the top panel). (b, c) Mean values of peak amplitude and frequency recorded from neurons. Unlike CMP group, CMP-ES group showed obviously increased AP peak amplitude and frequency. (d) Percentage of neurons showing repetitive Aps under different culture conditions. A total of 42 (5/12), 30 (3/10) and 53% (8/15) of recorded neurons on PDL, CMP, and CMP-ES, respectively, fired mature APs. (e) Peak AP amplitude significantly reduced by TTX. (f) Traces of spontaneous synaptic currents recorded from NSC derived neurons of PDL, CMP, and CMP-ES groups under voltage-clamping at −70 mV, scale bars: 20 pA and 1s. (g, h) Peak amplitude and frequency data produced by neurons on PDL, CMP, and CMP-ES. Numbers above bars indicate total number of cells examined from at least three independent cultures. Significant differences between CMP and CMP-ES results are marked. (i) Distributions of peak amplitude of spontaneous synaptic currents from different groups. CMP-ES group has higher current points and a more uniform frequency distribution than the CMP group. *$p < 0.05$, **$p < 0.01$ and ***$p < 0.001$.

could flow through the circuits formed between the neurons and the conductive substrate, triggering intracellular Ca^{2+} influx and Ca^{2+} release in addition to voltage-gated Ca^{2+} influx. Intercellular Ca^{2+} flow might also have been present. This set of results further confirm that ES can facilitate the electrophysiological maturation of NSC-derived neurons.

2.4. RNA-seq investigations on NSC differentiation under ES

RNA-seq was used to explore the potential molecular mechanisms mediating the biological behaviours of NSCs in response to ES. The initial bioinformatics analysis was performed on differentially expressed genes (DEGs). Using the K-Means Clustering algorithm, three distinct gene expression patterns, corresponding to clusters I, II and III, were identified on day seven. Using the gene lists in STable 1, Sheet 1, a total

of 2,361, 764 and 1405 genes were found to be specifically expressed in the CMP-ES, CMP, and PDL groups, respectively (P-value < 0.05, two-tailed *t*-test) (Fig. 5A). The genes in the CMP-ES group were involved in the 'Axonogenesis','Nervous system development', 'Endosome transport','Wnt signalling', 'MAPK signalling' and 'Neurotrophin signalling' and 'mTOR sinaling' pathways of biological processes, which promoted neuronal survival, axonal growth and differentiation (Fig. 5B). Meanwhile, the Biological processes of 'Cellular protein metabolic process', 'Cellular protein catabolic process' and 'Response to endoplasmic reticulum stress' was known to have the interplay with the autophagy pathway [37,38]. Besides, the enriched molecular GO pathways of 'Ubiquitin mediated proteolysis', 'MAPK signaling pathway',

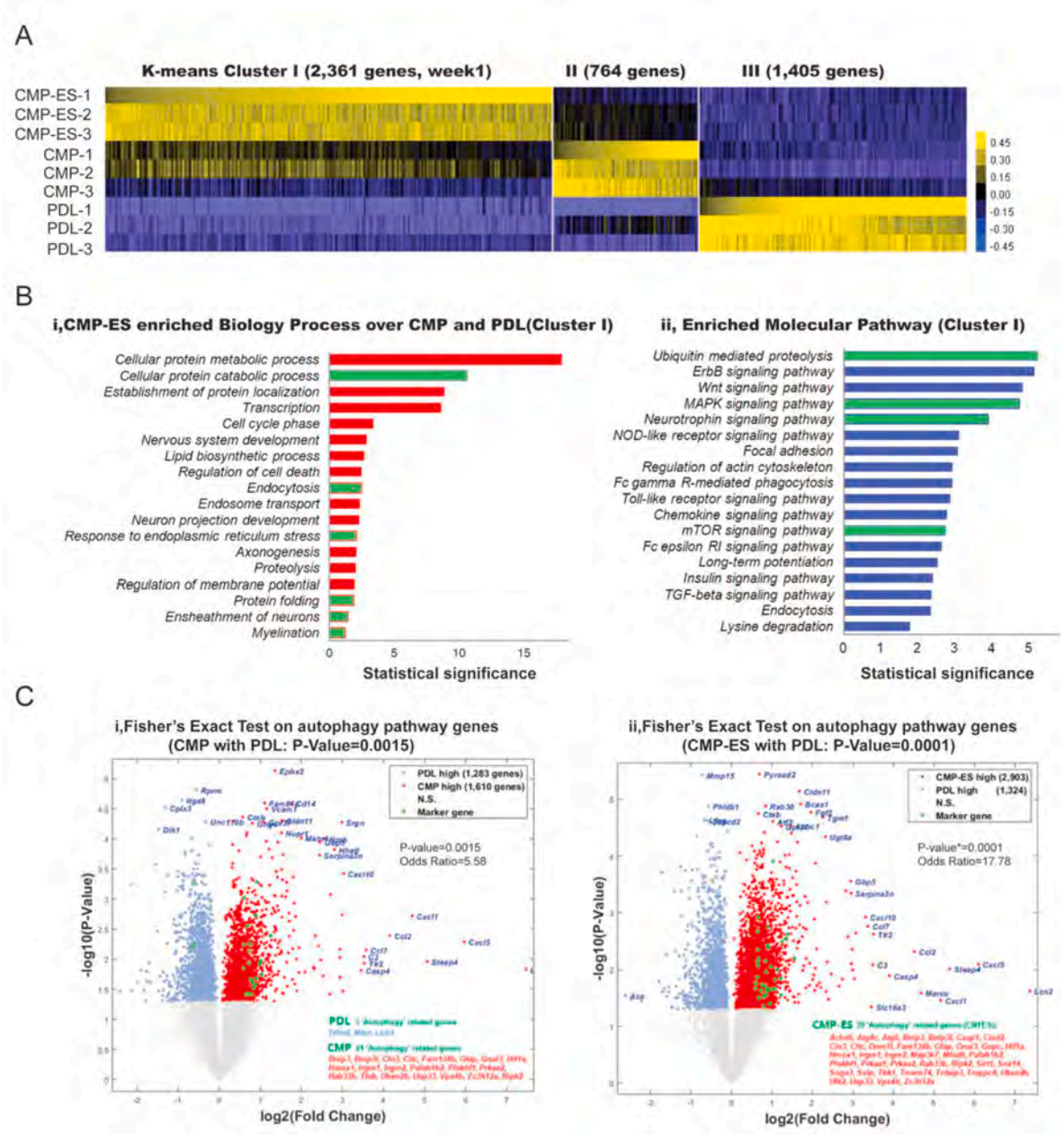

Fig. 5. Unsupervised and supervised analyses showed that the Biology Processes and Molecular Pathways of 'autophagy' were enriched for the cluster of genes that were upregulated under ES condition, and were associated with the processes and pathways that regulate 'nervous system development' and 'neuron differentiation'. (a) Unsupervised K-means clustering analyses showed that 2362, 764 and 1405 genes were specifically expressed in the cells that were cultured under the CMP-ES, the CMP and the PDL condition, corresponding the cluster of I, II and III. (b) The CMP-ES cluster I genes played the specific roles in regulating the autophagy related processes and pathways, including 'Protein catabolic process', 'Endocytosis', 'Response to endoplasmic reticulum stress', 'Ubiquitin mediated proteolysis' and 'mTOR signaling' (green bars). The Biology Processes and Pathways that occurred in all the 3 types of cell were shown in red and blue bars. They contributed to 'Nervous system development', 'Neuron projection development' and 'Neurotrophin signaling activity', suggesting that the 'autophagy' pathway was activated through ES, and interacted potentially with the 'ER stress response' and 'cell death' gene regulatory programs for neural cell stress adaptation, survival and differentiation. (c) Supervised analyses by retrieving the known autophagy-related genes from GO term database indicates that the autophagy pathway genes were significantly over-represented in the geneset of CMP-ES compared to PDL, as shown in the 2 Volcano plot on the right panel, where Fisher's Exact Test P-Value = 0.0001 and Odds Ratio = 17.78. While, under the CMP condition without any ES, the P-Value and Odds Ratio are less significant statistically, with P-Value = 0.0015 and O.R. = 5.58, suggesting that ES may further enhance the activity of autophagy pathway and boost Neural Stem Cell differentiation and maturation. (For interpretation of the references to color in this figure legend, the reader is referred to the Web version of this article.)

'Neurotrophin signaling pathway' and 'mTOR signaling pathway' also played the roles in the cross-talk and regulating cell autophagy [39–42]. Further pairwise comparison revealed 1610 and 2903 genes that were up-regulated under the CMP and CMP-ES conditions over PDL, respectively (STables 3 and 4; Sheets 1, 2, 5 and 6). Of the genes with greater than 1.5-fold differences, the 'Autophagy' process-related genes, shown in green solid circles in Fig. 5C, were significantly over-represented in the CMP group. Note that the genes that are well known to regulate autophagy (Atg4c, Atg5, Acbd5, and Ulk2) were significantly up-regulated following ES treatment. Autophagy is involved in the regulation of homeostasis and neurogenesis in neural stem cells (NSCs) [43]. Further GO term analysis with a pairwise comparison gene set further confirmed that the 'Autophagy', 'MAPK signaling', 'Vesicle-mediated transport', 'Regulation of neurogenesis', 'mTOR signaling', 'Neurotrophin signalling' and 'Lysosome' pathways were detected with higher enriched in the CMP-ES group; the green bars in SFig.5 highlighted the biological processes and molecular pathways that were most specifically over-represented (STables 3, 4; Sheets 3, 4, 7, and 8). These results are consistent with the results of the pairwise comparison between the cells in the CMP-ES and CMP groups, which showed that the genes in the CMP-ES group that regulate 'autophagy lysosome formation', 'Axon guidance' and 'Neurotrophin signalling' were significantly up-regulated relative to those in the CMP group (SFig. 6; STable 5; Sheets 1, 2, and 3). Collectively, these results suggest that ES can promote neurogenesis, neural differentiation and survival through the modulation of an 'autophagy'-coordinated transcriptional gene regulatory network (GRN).

Intriguingly, fewer DEGs were involved in the autophagy pathway at day 14, with the expression more down-regulated in the CMP-ES group than in the PDL group, suggesting that the autophagy gene regulatory programme might have reached an adaptation stage or become less involved. Using K-Means clustering, 821, 231, and 2324 genes were identified to be specifically up-regulated in the CMP-ES, CMP, and PDL groups, respectively, as shown in the heatmap in SFig.7A. GO analysis results indicate that the cluster I genes activated in response to ES played the roles of regulating the 'Cell-matrix adhesion', 'Neurotrophin signaling pathway', 'Protein modification process', and 'Integrin-mediated signaling pathway' pathways, which are required for the establishment of cell-cell and cell-ECM interactions and have significant impact on the survival, growth and terminal differentiation of neural cells (SFig. 7B). Volcano plots of the DEGs of the NSCs in the CMP and CMP-ES groups versus those expected on the PDL group (SFig.7C) indicate that these genes regulated the autophagy process but were not statistically overrepresented in the CMP or CMP-ES groups (two-tailed Fisher's exact test; p-values = 0.636 and 0.559, respectively) relative to the PDL group. GO term analysis revealed enriched biological processes and molecular pathways in 'Focal adhesion', 'ECM-receptor interaction', 'Cytokine-cytokine receptor interaction', 'Integrin signaling pathway', 'Axon guidance', 'Neurotrophin signaling pathway', 'Neuron projection morphogenesis', and 'Regulation of neuron differentiation', which suggests that the cells might have reached a terminally differentiated stage and/or adapted themselves to stress (SFig. 8; STable 7; Sheets 2 and 3).

2.5. ES enhanced autophagy of NSC-derived neurons

Recent studies have identified the involvement of autophagy-related genes (Atg) in NSC differentiation, implicating the regulation of autophagy in NSC neurogenesis [22,23,44]. However, the underlying mechanism has not been thoroughly illuminated. Given that the PI3K/Akt and mTOR signalling pathways, the main regulators of autophagy, were significantly enriched following the administration of ES in our experiments, we sought to identify whether ES stimulated neuronal autophagy. Following cultivation for 7 d in the differentiation medium, NSC-derived neurons of the CMP-ES group demonstrated significantly increased populations of LC3B puncta, a classic marker of autophagosomes, relative those of the PDL and CMP groups (Fig. 6A and B), and the mRNA levels of the CMP-ES group LC3B and Atg 3 were higher than those of the CMP group (Fig. 7C). ES treatment also promoted lipidation of LC3B (a change in the ratio of LC3B-II/LC3B-I) and decreased the expression of p-mTOR (ser 2448) and p-ULK1 (ser 757) (Fig. 6D and E). These data suggested that ES probably activated autophagy by suppressing the mTOR signalling pathway.

After 14 d of cultivation, the number of LC3B puncta in the neurons of the CMP-ES group was also increased relative to the other two groups (Fig. 6F and G). However, the differences in the autophagy markers and mTOR signalling pathways, as determined by polymerase chain reaction (q-PCR (H)) and Western blot analysis, were not significant among the three group samples (Fig. 6 I, J), possibly as a result of the compensation effect of the proliferation of differentiated gliocytes produced by the NSCs, which, through their enhanced numbers, could have resulted in a higher level of autophagy than was produced by the neurons. We then went back to examine the autophagy level at day 10. As shown in SFig. 9, increased levels of LC3-II and Lamp 1, along with an increased lipidation of LC3B, were clearly observed in the CMP-ES groups. These results suggest that autophagy played an important role in the ES-induced neuronal differentiation process of the NSCs.

2.6. Autophagy plays a crucial role in ES-induced neuronal differentiation and functions

To precisely determine the effects of autophagy on the neuronal differentiation and functions of NSCs under ES, we performed autophagy activation and inhibition by treating cells with rapamycin (autophagy activator) and Ly294002 (autophagy inhibitor) at the same time as the ES treatment (SFig.10A). As shown in Fig. 7A, rapamycin treatment indeed enhanced autophagy at day seven, as revealed by the increased level of LC3-II staining and lipidation of LC3B. By contrast, treatment with Ly294002 decreased the level of LC3-II staining and lipidation of LC3B and, therefore, suppressed autophagy. We then examined whether drug treatment would affect neuronal growth. The morphological analysis results demonstrated that (Fig. 7C–F), when cells cultured on different substrates, the neurite length and branch number per cell of CMP-ES group were significantly higher than those of the CMP group. Following rapamycin treatment, the neurite length and branch number of PDL and CMP-ES group did not show much different than the control one, while those in CMP group had a little bit increment, which let the four indicators have no significant difference between CMP group and CMP-ES group. When Ly294002 treatment was applied to the NSC-derived neurons, the neurite length and branch number of all three groups decreased, especially the longest neurite length per cell, both CMP group (107.5 ± 64.497 μm), and CMP-ES group (111.589 ± 70.592 μm) have reduced to almost half of that in PDL group (212.544 ± 81.254 μm). And similarly, there was no significantly difference in each index during CMP group and CMP-ES group. Besides, Ly294002 treatment had significant effects on NSC-derived neurons, with the density decreasing in the PDL group. As a novel autophagy inhibitor, Ly294002 inactivates Akt/PKB, thereby inhibiting cell proliferation and inducing apoptosis [45]. However, the density of NSC-derived neurons showed only a slight decrease in the CMP group and no significant decrease in the CMP-ES group in response to Ly294002 treatment. These observations indicated that the nano-scaled substrate produced by the CNT multilayers provided a permissive environment for neuron survival and that the use of ES further promoted neuron viability. Overall, autophagy was found to play a critical role in the viability and neurite outgrowth of neurons differentiated from NSCs under ES.

We then examined effects of the rapamycin and Ly294002 treatments on the electrophysiological functions of NSC-derived neurons at day 14 along with ES treatment (SFig. 10B). The rapamycin treatment was found to consistently increase the level of LC3-II staining and the lipidation of LC3B, while treatment with Ly294002 decreased the level of LC3-II staining and the lipidation of LC3B (Fig. 8A). Then, patch

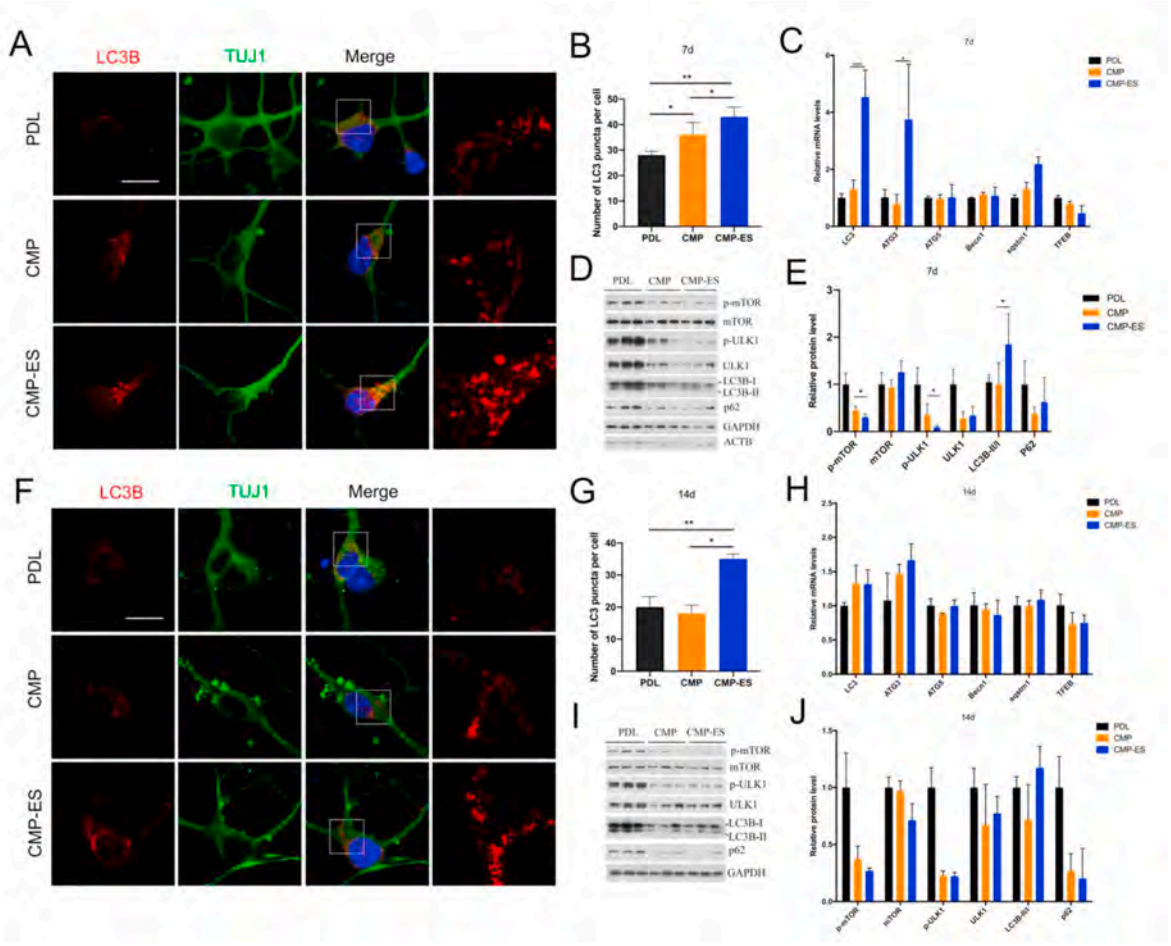

Fig. 6. ES treatment-enhanced autophagy. (a) Representative immunofluorescence images of LC3B puncta and respective quantitative results for (b) neurons in PDL, CMP, and CMP-ES groups at day seven. (c) qPCR of autophagy-related genes in all three groups at day seven. (d) Representative western blots and (e) quantitative densitometric results of mTOR signaling pathway proteins and LC3B in all three groups at day seven. (f) Representative immunofluorescence images of LC3B puncta and (g) respective quantitative results for neurons in PDL, CMP, and CMP-ES groups at day 14. (h) qPCR of autophagy-related genes in all three groups at day 14. (i) Representative western blots and (j) quantitative densitometric results of mTOR signaling pathway proteins and LC3B in all three groups at day 14. *$p < 0.05$, **$p < 0.01$. Scale bars = 20 μm.

clamp was used to verify the drug treatment effecting on electrophysiological activity. As shown in Fig. 8, the frequency and peak amplitude of APs in the CMP-ES group were significantly higher than the CMP group in the control condition. Following rapamycin treatment, the higher peak amplitude and more frequency had been created in the CMP group but not in the PDL and CMP-ES group, which made no statistical difference between CMP and CMP-ES group. The proportion of cells treated with rapamycin that were capable of triggering intact APs was significantly increased (50%, versus 37 and 33%, respectively) relative to the control and Ly294002 groups (Fig. 8E). While the Ly294002 treatment resulted in decreased neuronal viability proportion and a reduction in the number of cells capable of firing APs relative to the other two groups (Fig. 8B–E). In addition, following addition of Ly294002, the frequency and peak amplitude of APs in the CMP-ES group were significantly lower than the control one (Fig. 8C, D). In all three group, the peak amplitude and frequency of APs remarkably decreased after Ly294002 treatment, revealing that the electrophysiological activity was suppressed by inhibiting autophagy. Collectively, these results further suggest that autophagy plays an important role in process through which ES promotes neuronal functional maturation.

2.7. Autophagy manipulation of neurite outgrowth can be regulated by ES and drugs

To further analyse the effects of ES on the autophagy of NSC-derived neurons, we increased the ES current to 2 mA. As shown in Fig. 9A, the expression of the intracellular autophagy marker LC3B in the neurons was significantly increased at day seven relative to the 1 mA treatment results. In addition to accumulation within the neuronal soma, abundant LC3B-positive autophagosomes were found to be distributed along the neurites. However, the neurite outgrowth of the NSC-derived neurons was seriously depressed, as characterised by the diminished neurite length (Fig. 9B–D) and degree of branching (Fig. 9 E) along with the poor neuronal growth states caused by fractured neurites when increased ES current from 1 mA to 2 mA. Interestingly, following Ly294002 treatment, the long neurites of 2 mA treatment, with numerous branches and characteristics comparable to those at an ES current of 1 mA without drug treatment, reappeared. Neuronal autophagy was significantly suppressed as a result of Ly294002 administration, which instead improved neuronal viability. These results suggest that the autophagy was closely related to neurite outgrowth. Autophagy is an important intracellular process that maintains intracellular energy and homeostasis [46], and proper ES is required to ensure moderate autophagy and the effective manipulation of neuronal fate. Applying ES at current levels that are too high can cause excessive

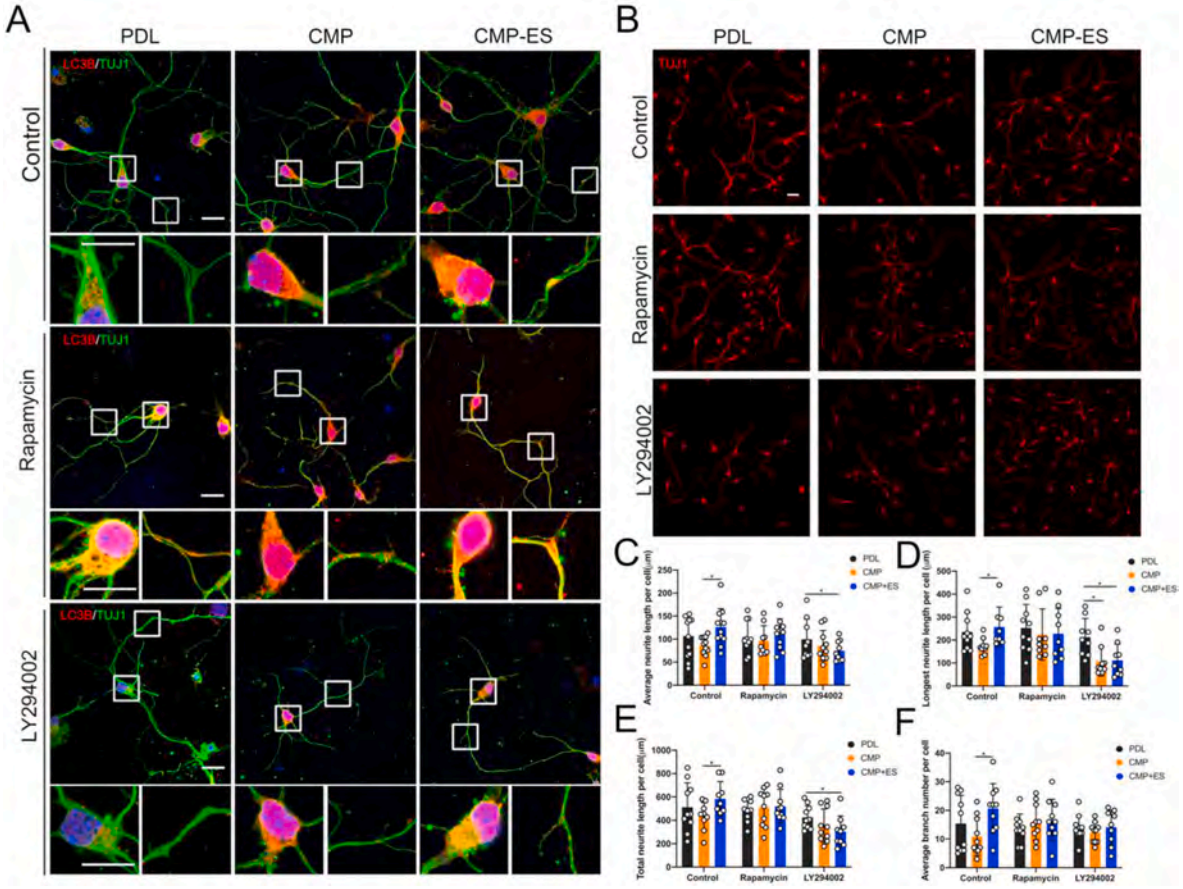

Fig. 7. Cell morphology and morphological analysis of NSC-derived neurons following treatment with autophagy activator (rapamycin) or inhibitor (Ly294002). (a) Representative images of cellular immunostaining following treatment with rapamycin or Ly294002. The rapamycin treatment increased the level of LC3-II staining and the lipidation of LC3B, while Ly294002 treatment decreased the level of LC3-II staining and the lipidation of LC3B. (rapamycin, 1 μg/ml, Ly294002, 25 μM) Scale bar = 20 μm. (b) Representative immunofluorescence staining of NSC-derived neurons at day seven. The average neurite length (c), longest neurite per neuron (d), total neurite length per cell (e), and average branch number (f) were quantitatively analysed. n > 6, $*p < 0.05$ and $**p < 0.01$. Scale bars = 50 μm.

autophagy, leading to imbalances and deteriorating neuronal biological behaviours. Restoring the balance by, e.g., administering an autophagy inhibitor, can effectively improve neuronal behaviour. The schematic diagram in Fig. 9F summarizes the findings of this study. Essentially, ES can trigger the inflow of calcium ions, which in turn activate multiple signalling pathways, including PI3K/AKT/CREB signals, autophagy and mTOR signalling pathways.

3. Discussion

NSCs have been shown to hold significant promising and peculiar therapeutic plasticity in the treatment of severe CNS diseases and injuries by restoring connectivity through the induction of new relay circuits in lesions. Treatments or trainings of NSCs prior to transplantation have been performed to promote the efficacy of NSC neurogenesis [7,8]; among such treatments, ES has been shown to exert exogenous electrical signals that enable the effective manipulation of NSC fate by mimicking the action potentials of the CNS. In this study, new multichannel ES device was applied to promoted NSCs differentiation into mature neurons. ES at nanoscale topography could activate autophagy to promote neuronal differentiation, which is conducive to the survival of exogenous NSCs, and also provides the precondition NSC-derived neurons with high-level autophagic activity, healthier and more energetic for transplantation in vivo and improved the transplant survival efficiency.

The ES setups used in previous studies, however, were designed for use on exploratory lab benches. In most cases, a single customised cell chamber was mounted onto conductive film and two electrodes were attached to the conductive substrate outside of the chamber [15,47,48]. Some researchers placed conductive films in the wells of the cell culture plates and then directly connected electrodes to the wells in close contact with the films [49,50]. As setups such as these were handmade, there were large variances in the parameters of each chamber or batch. The applied electric current and field were likely to fluctuate, resulting in poor stability and ES reliability and presenting barriers to scaling up for cell treatment. Furthermore, the use of metal electrodes produced a risk of electrolysis of the cell culture medium. In this study, we used a specifically designed ES system (Fig. 1A) that could supply stable current to NSCs cultured on CNT-multilayered substrates for cell treatment on a large scale. The use of CNT multilayers with nano-scaled topography provided a permissive environment for the development of focal adhesions, thereby facilitating neural attachment [35].

Administration of ES further enhanced the interactions between the NSC-derived neurons and substrates, as indicated by the production of abundant filopodia and lamellipodia structures within the growth cones and along the neurites (Fig. 2E–H). Neuronal growth cones act to guide growing neurites to appropriate locations for establishing correct interconnection and transmit information. Through this growth patterning, neurite outgrowth was promoted by the ES, resulting in an increase in neurite elongation and branching, which in turn facilitated neuronal cytoarchitecture complexity. Through these mechanisms, ES appeared to promote neuronal maturation, as was further confirmed by increases in the expression of NeuN, and the secretion of BDNF, a potent target-derived protein favouring neural communications. Furthermore, the electrophysiological functions of the NSC-derived neurons were

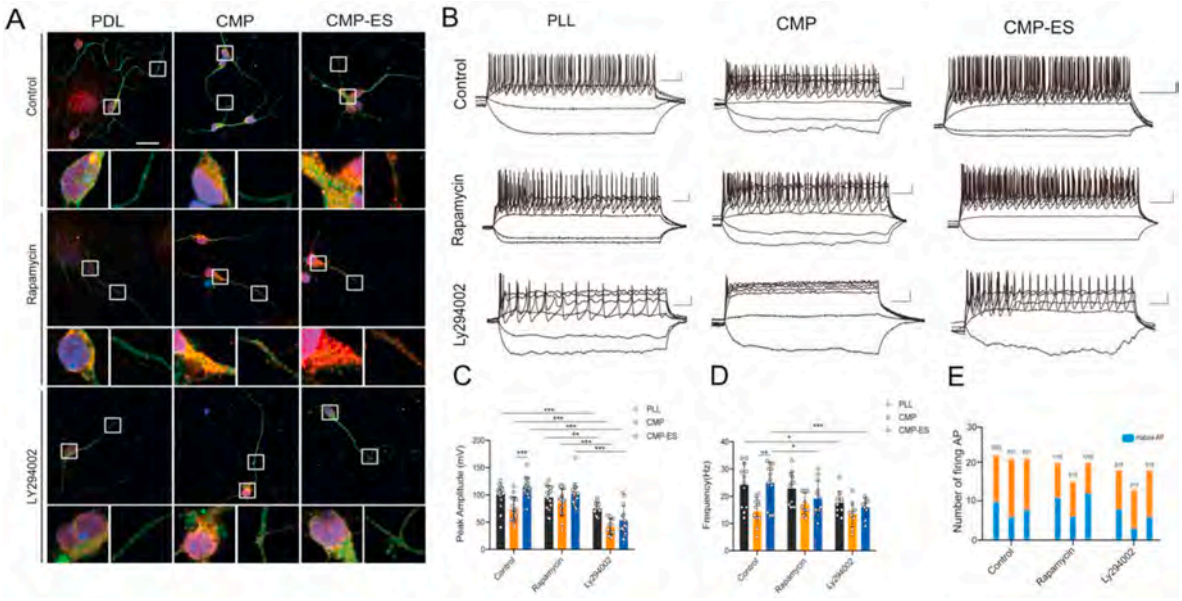

Fig. 8. Functional maturation of NSC-differentiated neurons following treatment with rapamycin or Ly294002. (a) Representative images of cellular immunostaining following treatment with rapamycin or Ly294002. Rapamycin treatment increased the level of LC3-II staining and the lipidation of LC3B, while Ly294002 treatment decreased both. (b) Representative trace of repetitive APs produced after addition of rapamycin and Ly294002. From top to bottom, the images show control, rapamycin, and Ly294002 groups, respectively. Scale bars: 20 mV and 50 ms. (c, d) Summary of peak amplitudes and frequency of differentiated neurons under different treatment conditions. Data shown as mean ± SD. (e) Numbers above bars give total number of cells examined from at least three independent cultures. Significant differences are marked *$p < 0.05$, **$p < 0.01$ and ***$p < 0.001$.

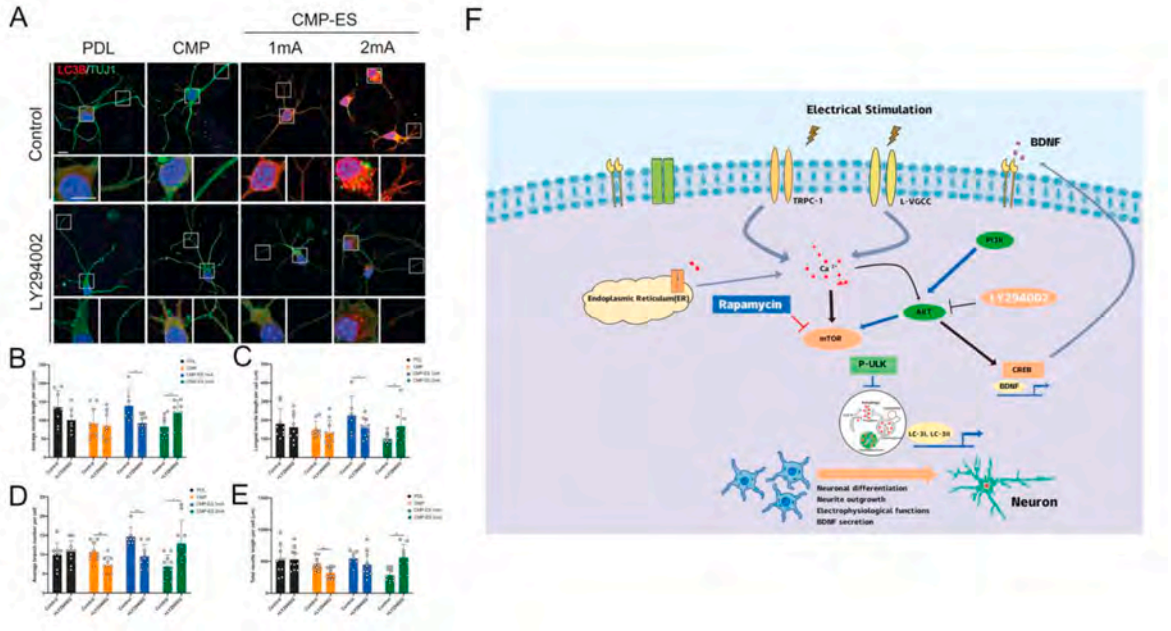

Fig. 9. Autophagy of NSC-derived neurons at day seven under different ES currents. (a) Representative images of cellular immunostaining of autophagy markers LC3B following treatment with the autophagy inhibitor LY294002. Increasing the ES current to 2 mA increased the expression of intracellular autophagy marker LC3B to an excessive degree, resulting in lower average neurite length (b), longest neurite per neuron (c), average branch number (d) and total neurite length per cell (e) than under 1 mA ES. Adding the autophagy inhibitor lowered the activation level of autophagy, restoring the values of various neurite indicators. *$p < 0.05$, **$p < 0.01$, ***$p < 0.001$. Scale bars = 20 μm. (f) Schematic diagram summarizes the findings of this research. ES can trigger the inflow of calcium ions, which in turn can activate multiple signaling pathways, including PI3K/AKT/CREB signals, thereby promoting BDNF secretion. It can also activate autophagy by suppressing the mTOR signalling pathway, which plays a crucial role in the neuronal differentiation process of NSC-derived neurons. Application of autophagy activator (rapamycin) and inhibitor (Ly294002) can regulate the autophagy activity to manage neuronal viability, neurite outgrowth, and maturation of NSC-derived neurons.

found to be significantly enhanced by ES, as indicated by their capability of firing repetitive APs with various electrophysiological parameters specific to mature neurons. The presence of robust spontaneous synaptic events suggested the formation of functional synapses with other neurons. Overall, ES promoted NSC differentiation into neurons of high maturity and electrophysiological functioning in the absence of the

chemical agents typically required for neurogenesis.

Despite a number of recent studies focusing primarily on cytoskeletal microfilament recombination, cell-surface receptor redistribution, changes in intracellular Ca^{2+} dynamics, etc. [51], that have looked at the potential effects of ES on NSCs, the critical mechanisms remain incompletely understood. In this study, the RNA sequencing was used to explore the potential mechanism underlying neuronal differentiation and functional maturation of neuron in response to ES. Further GO term analysis with a pairwise comparison gene set confirmed that ES induces significantly enriched autophagy-associated genes, biological processes and molecular pathways of NSC-derived neurons, confirming the presence of autophagy signaling (Fig. 5, SFig.5). As a basic cellular response to stress, autophagy can be assumed to play a critical role in the cellular homeostasis and neurogenesis of NSCs [43]. Knockout of Atg5 or other autophagy-related-gene FIP200 impaired neuronal differentiation of NSCs in sub-granular zone (SGZ) of the dentate gyrus (DG) by reducing new-born neuron numbers and neuronal maturation [52,53]. During the neurogenesis, the expression of Atg9a levels and the LC3-II/LC3-I ratio (a readout of autophagy) increased in NSPCs derived from the forebrain. Overexpression of Atg5 in mice induces autophagy and prolongs the lifespan and is associated with anti-aging phenotypes including leanness, increased insulin sensitivity, and improved motor function [54]. Our finding from this study on one hand demonstrated that ES treatment upregulated lipidation of LC3B and downregulated the expression of p-mTOR and p-ULK (Fig. 6), on the other hand autophagy of NSC-derived neurons can be significantly enhanced in the manipulation of NSC neurogenesis following an effect similar to that produced by rapamycin, a typical autophagy activator (Figs. 7 and 8).

Autophagy not only regulates neurogenesis but also implicates in controlling synaptic strength and plasticity [55]. Autophagic activity is essential for BDNF-induced synaptic plasticity in regions of the mouse forebrain [41]. Developmental spinal pruning requires mTOR-regulated autophagy, and the activation of neuronal autophagy could correct synaptic pathology and social behavior defects in autism spectrum disorders (ASD) models [56]. Pharmacological inhibition of autophagy with wortmaninn or 3-MA (PI3K inhibitors) markedly prevented neuronal differentiation of NSPCs resulted in a low survival rate of NSPCs and undermined self-renewal capacity of NSCs [20]. In this study, following Ly294002 treatment, the neurite length, branch number and numbers of firing APs remarkably decreased in all three groups (Figs. 7 and 8), and also affecting neural viability. Further increases in the ES current were found to robustly enhance autophagy but cause poor viability of NSC-derived neurons, deteriorated electrophysiological functions and severe neurite outgrowth (Fig. 9). Suppression of autophagy by an inhibitor was found to decrease autophagy but restore cell viability, neurite outgrowth and electrophysiological functions to their previous levels.

Compared with cultivation for 7 d, there was no significant differences between the autophagy markers and mTOR signaling pathways among the three group at day 14 (Fig. 6), possibly due to compensatory effect on the proliferation of differentiated gliocytes produced by the NSCs, which, through their increased numbers, could have resulted in a higher level of autophagy than was produced by the neurons. Previous studies suggested that microglia autophagy is also important in synaptic refinement and maturation of neuronal connections of normal brain development [57,58]. Autophagy in microglia has an important role in regulating synaptic homeostasis and neuropsychological behaviors in ASD model [58]. Microglia may select synapses to be pruned based on firing patterns and synaptic strength, as described for the neuromuscular junction and retinogeniculate synapse [59] and require autophagy for the degradation of this material, whereas neuronal autophagy may be required for intrinsic neuronal mechanisms of structural plasticity [55,60].

To our knowledge, these findings represent the first evidence that the regulation of autophagy primarily through mTOR signaling is an important acting pathway in the process through which ES promotes neuronal differentiation and the maturation of NSCs. It is tempting to propose a mechanism through which ES exerts stimulus pressure to NSC-derived neurons to activate autophagy-related signaling events that regulate their important biological processes. The results of this study contribute to the theoretical advancement of ES for modulating NSC performance to obtain better therapeutic outcomes, with the results presenting an improvement over conventional strategies involving cytokines, which are complicated, expensive and unstable. Furthermore, profound insights have been provided for the future application of ES, individually or in combination with autophagy-regulating drugs, in NSC-based strategies for neural regeneration.

4. Methods

4.1. Preparation of CNT-multilayered nanocomposites (CMP)

The CNT-multilayered nanocomposite fabrication protocol is reference to our previous research [24,25]. Briefly, a total of 100 mg of CNT-COOH was dissolved into 500 ml of ultrapure water via sonication for 2 h to prepare the CNT-COOH solution. Prior to the fabrication, quartz substrates were dipped into PEI solution for 30 min to obtain a positively charged surface. The PEI-activated quartz substrates were then immersed into the CNT-COOH suspension and a PDDA solution (2.0 mg/ml in ultrapure water) for 20 min each. Each step was followed by washing three times with water. The cycle was repeated 10 times to obtain the CNT-COOH/PDDA multilayered films (CMP).

4.2. Multi-channel ES device

In this study, we utilized a popularly microcontroller unit (MCU) commands and developed a multi-channel ES platform that accommodates simultaneous application of multiple ES parameters with an interactive touch screen [27]. It consisted of a 6-channel current digital to analog converter (DAC) as the source of ES and each channel had an independent current output. Stimulation frequency ranged from 0 Hz to 100 kHz, with intervals of 1 Hz and the resolution of the current amplitude adjustment was 10 bits. The wide selection range enabled experiments on most human cell tissues. With a fully embedded system, only a portable general power supply was needed to power the system. Unlike the traditional setup, which heavily relied on a bulky generator, this tool opened up the possibility of examining many dependent variables, such as temperature and radiation exposure, with ease of use. Electrodes used in this system were chemically inert carbon material to sustain a long shelf-life. Using an oscilloscope to display the changes of voltage and current during ES. Briefly, put ES device into the 24 well culture cell plate, connected the line of the stimulation device to the controller, set the relevant parameters, and connected the oscilloscope wire with the controller. Then, the data on the oscilloscope can be seen in the process of ES. The current and voltage in the culture dish would be shown on the oscilloscope, which can effectively reflect the reliability and advancement of the equipment.

4.3. NSCs culture and electrical stimuli

NSCs were isolated from the whole brain of embryonic day-14.5 (E14.5) female C57 mice (Guangdong Provincial Animal Centre). Tissues were digested with 0.15% Trypsin/EDTA incubated in a 37 °C water bath for 7 min, after which a 10 mg/ml Trypsin Inhibitor and 30 KU/ml DNase I (working concentration 150 U/ml) and 15 μl of 1 M $MgCl_2$ (working concentration 10 mM) were added and mixed for 1–2 min to neutralise the trypsin and digest the released genomic DNA. Following filtration and centrifugation, isolated cells were obtained.

Primary NSCs were cultured at a concentration of 1×10^5 cells/cm^2 in a 25 cm^2 culture flask (Corning, USA) at a final volume of 5 ml in Dulbecco's modified Eagle's medium Nutrient Mixture F-12 (DMEM/F12, Gibco, USA) supplemented with 1% EGF (Gibco, USA), 1% bFGF

(Gibco, USA), 1% N2 supplement (Gibco, USA), 1% GlutaMAX-I (Gibco, USA), 2% B27 supplement (without Vitamin A) (Gibco, USA), 0.1% heparin (MCE, HY-17567A) and 1% penicillin-streptomycin (Gibco, USA) in a 5% CO_2-humidified chamber (Thermofisher, USA) at 37 °C. The NSCs were passaged approximately once per week and, at passage two (P2), the cells were digested with StemPro Accutase (Thermofisher, USA) into isolated cells and then seeded onto PDL or CMP substrates at a concentration of 7×10^4 cells/cm^2. Single NSCs were cultured in a differentiation medium comprising DMDM/F12 supplement with 2% B27 supplement (Gibco, USA), 1% penicillin-streptomycin and 1% fetal calf serum (Gibco, USA).

We performed electrical stimulation for 3–5 d in a 7-d cycle. The electrical stimulation conditions were determined to be 20 Hz, 1 mA and 2 h per day (the experimental device was provided by Professor Cui of the Hong Kong University of Science and Technology).

4.4. Immunofluorescence detection

The NSCs were fixed with 4% formaldehyde and incubated with Mouse anti-mouse βIII-Tubulin (1:1000, Abcam, UK); Mouse anti-mouse DCX(1:1000, Abcam, UK); Rabbit anti-mouse MAP2 (1:1000 , Abcam, UK); Mouse anti-mouse NeuN and Rabbit anti-mouse PSD95 (1:1000, Abcam, UK); Rabbit anti-mouse GAP 43 antibody(1:800, Abcam, UK); Alexa Fluor 488-phalloidin(1:800, Invitrogen, USA, UK); and Goat anti-rabbit LC3B(1:200, Sigma, L7543). Donkey Anti-Mouse IgG H&L (Alexa Fluor® 555) (1:1000, Abcam, UK) or Donkey anti-rabbit IgG H&L (Alexa Fluor® 488) (1:1000, Abcam, UK) were used as secondary antibodies. Nuclei were counterstained with DAPI. Slides were viewed using a Zeiss LSM 710 Confocal Microscope (Zeiss, Germany). Then, the gray value of each pixel represents the fluorescence intensity of that point which was measured by ImageJ software, the formula of fluorescence intensity in a specific area was: Mean gray value = Integrated Density/Area. At last, export the fluorescence intensity of the three groups to excel, use the GraphPad for more analysis.

4.5. Neuronal cytoskeleton 2D construction

A two-dimensional cytoskeleton of the neurons differentiated from the NSCs, which were labelled with β III-tubulin, was constructed using Neurolucida software. Concentric circles mark the distance between the protrusion and the cell body, and the adjacent concentric circles were separated by 10 μm. The colors on the neurites reconstructed by Neurolucida software were divided by branch points, different colors represent branches of different grades , the color can be defined through the software. The lengths and branch numbers of the axons and dendrites of the neurons were quantitatively analysed.

4.6. RNA extraction and quantitative real-time PCR analysis

Total RNA was extracted from the cells using an RNA extraction kit (DongSheng, China), following the manufacturer's recommendations. The total RNA (1 μg) was then used for reverse transcription (RT) via a commercially available kit (PrimeScript RT reagent Kit with gDNA Eraser, TAKARA, China). Real-time PCR was performed in triplicate with an ECO system (Gene Company Limited, HK, China) and a fluorescence-labelled SYBR Green qPCR Master Mix kit (TAKARA, China) using specific primers. With 18S rRNA taken as an endogenous control DCX, βIII-Tubulin, MAP2, NeuN, PSD95, LC3B, ATG3, ATG5, BECN1, SQSTM1 and TFEB were detected (the primer sequences are listed in Table 1). The results were analysed using the ECO software (Gene Company Limited, HK, China), with gene expression calculated from the accurate threshold cycle (Ct), which is the PCR cycle at which an increase in the fluorescence from SYBR Green probes above the baseline signal can first be detected. The Ct values for the 18S rRNA were compared with those from DCX, βIII-Tubulin, MAP2, NeuN, PSD95, LC3B, ATG3, ATG5, BECN1, SQSTM1 and TFEB in each well to calculate ΔCt. Data corresponding to the treated conditions were expressed relative to the signal obtained as the average of the untreated controls via ΔΔCt calculation. The triplicate ΔΔCt values for each sample were averaged.

Table 1
Primer sequences used for qRT-PCR.

Gene name	Forward(5'→3')	Reverse(5'→3')
18S rRNA	GTAACCCGTTGAACCCCATT	CCATCCAATCGGTAGTAGCG
DCX	CATTTTGACGAACGAGACAAAGC	TGGAAGTCCATTCATCCGTGA
βIII-Tubulin	TAGACCCCAGCGGCAACTAT	GTTCCAGGTTCCAAGTCCACC
MAP 2	ATGACAGGCAAGTCGGTGAAG	CATCTCGGCCCTTTGGACTG
Rbfox3 (NeuN)	ATCGTAGAGGGACGGAAAATTGA	GTTCCCAGGCTTCTTATTGGTC
PSD95	CCTGTCGGTCAATGGTGT	CCTCGAATCGGCTATACTCT
LC3B	GCAAGAGGGGACCCTAACC	TTCTCCCCCTTGTATCGCTCT
ATG3	TGATCAACACGGTGAAGGGAA	TTCCCCTGTAGCCCTCTTCT
ATG5	ATGGACAGCTGCACACACTT	AGAGGGGTTTCCAGCATTGG
BECN1	CCAGCTGGACAAGCTCAAGA	CACTCCACAGGAACACTGGG
SQSTM1	ACTGCTCAGGAGGAGACGAT	AACCCATGGACAGCATCTGG
TFEB	TATCAGCTCCAACCCCGAGA	CTGTACACGTTCAGGTGGCT

4.7. Western blot analysis

Total proteins were extracted from the cells, with BCA reagent (Beyotime, China) used to measure the concentration of proteins. A total of 15 μg of protein samples was separated on a 10% polyacrylamide gel and transferred onto polyvinylidene fluoride membranes (Millipore, USA). Each membrane was blocked for 1 h with 5% defatted milk powder at room temperature and then incubated with DCX (Abcam, UK), β III tubulin (Abcam, UK), MAP2 (Abcam, UK), NeuN (Abcam, UK), PSD95 (Abcam, UK), LC3B (Sigma,L7543), p-mTOR (Ser 2448) (Cell Signaling Technology, 5536), p-ULK1 (Ser 757) (Cell Signaling Technology, 4202) or GAPDH (Cell Signaling Technology, 2118) primary antibody at 4 °C overnight. The blots were then washed three times with TBST and incubated with corresponding horseradish peroxidase-conjugated IgG secondary antibodies (Boster, USA) for 1 h at room temperature. The blots were developed in ECL chromogenic substrate (Millipore, USA) and the images were captured using a gel imager (UVITEC). The gray value of each band was measured using ImageJ (NIH, Bethesda, MD) software. The relative expression of each immunoreactive band was calculated by comparing the target protein band with GAPDH. There were six samples in each testing group, and each sample was tested three times.

4.8. Electrophysiological recording

Electrophysiological recording was carried out as previously described [61]. Whole-cell patch recording was performed using an EPC-9 amplifier (HEKA, Germany). The cells were transferred into a recording chamber at room temperature and filled with extracellular solution containing 126 mM NaCl, 2.5 mM KCl, 2 mM $CaCl_2$, 2 mM $MgCl_2$, 10 mM D-glucose, 1.25 mM NaH_2PO_4 and 10 mM HEPES at a pH of 7.3 and an osmolarity of 310 mOsm. The intracellular recording solution comprised the following: 130 mM K-Gluconate, 10 mM KCl, 2 mM $MgCl_2$, 1 mM $CaCl_2$, 10 mM EGTA, and 5 mM HEPES, 4 mM Mg-ATP and 0.4 mM Na_2-GTP, with a pH of 7.2 and an osmolarity of 310 mOsm. Fire-polished patch pipettes, ranging from 5- to 7-MΩ resistance, were used for all recordings. Action potentials were obtained using depolarisation pulses (0 pA for 100 ms in 1-s, 20-pA steps from −60 to +120 pA) and recorded under current clamp mode. Sodium and potassium currents were applied with a series of 60-ms voltage steps from −60 to 65 mV in 10-mV increments following a 100-ms pre-pulse to −100 mV. Voltage clamping at −70 mV was applied for 3–5 min to record spontaneous synaptic currents. Data were acquired using a HEKA amplifier at

a sample rate of 5 kHz, filtered at 3 KHz and then analysed using Patchmaster (HEKA) and Igor 5.2 (WaveMetrics, Lake Oswego, OR, USA), while spontaneous synaptic currents were analysed using the Minianalysis program designed by Synaptosoft Inc.(Decatur, GA, USA). All chemicals were obtained from Sigma.

4.9. Calcium imaging

Calcium imaging was carried out using the indicator Fura-2 AM, as developed previously, following two weeks of exposure of the NSCs to ES. The differentiated NSCs were loaded with 5-μM Fura-2 AM for 30 min at 37 °C in an atmosphere of 5% CO_2 and then washed three times with a normal bath solution containing 138 mM NaCl, 5 mM KCl, 0.3 mM KH_2PO_4, 4 mM $NaHCO_3$, 2 mM $CaCl_2$, 1 mM $MgCl_2$, 10 mM HEPES, and 5.6 mM Glucose at a pH of 7.4 and at 320 mosm/l at room temperature. Cover slips of the solution were placed on a Zeiss scanning microscope and superfused continuously at 2–3 ml/min. After combining with calcium ions, Fura-2 can produce strong fluorescence under 330–350 nm excitation light, and it caused fluorescence to decrease under 380 nm excitation light. In this way, 340/380 nm excitation ratio for Fura-2 allowed accurate measurements of the intracellular Ca^{2+} concentration. The fluorescence images were obtained at 5s intervals with minimal exposure during the course of the experiments. To induce calcium overload, neurons were exposed to electrical stimuli (20 Hz, 1 mA), with the fluorescent intensity ratio values calculated using Zeiss software. Briefly, opened data in ZEN blue, entered processing and select "Image calculator" in method, selected a series of data pictures, set channel one "Fura-2 340", other channel is "Fura-2 380", added the formula as Fura-2 340/Fura-2 380, then clicked "Mean ROI" tab, drew several ROIs on interesting cells, using ROI tools, obtained the plot of the relative fluorescence intensity change of the neurons during the ES time period. At last, exported the intensity ratio of the three groups to excel, used the GraphPad for more analysis.

4.10. ELISA analysis

The BDNF concentration was normalized to cell number following the ELISA kit protocol (Cloud Clone Corp, China). Neural stem cells (7×10^4 cells/cm^2) were cultured in the differentiation medium (DMEM/F12 supplemented with 2% B27, 1% penicillin-streptomycin sulfate and 1% fetal calf serum), and each group were treated as designed. Aliquots of the cell culture supernatants were removed on days 7 and 14 and assayed for levels of BDNF. The chromogenic reaction was monitored by measuring the absorbance at 450 nm in an EnSpire Microplate reader (PerkinElmer, USA).

4.11. RNA sequencing (RNA-seq) and identification of differentially expressed gene sets

Following NSC culturing in differentiation media for 7 or 14 d, the total RNA was isolated using Trizol and the integrity was evaluated using the Agilent 2200 TapeStation (Agilent Technologies, Santa Clara, CA). Each sample had an RINe above 7.0. mRNAs were isolated from the total RNA, fragmented to a size of approximately 200 bp and subjected to cDNA synthesis followed by adaptor ligation and enrichment with a low cycle using the TruSeq RNA LT/HT Sample Prep Kit (Illumina). The purified library products were evaluated using the Agilent 2200 TapeStation and Qubit 2.0 (Life Technologies), diluted to 10 pM for cluster generation in situ on the HiSeq 2500 Paired-End Flow Cell and finally sequenced (2×100 bp) on the HiSeq 2500 Platform (Illumina). Raw reads were filtered by removing those with adapters or contaminations or those with more than 10% N bases or more than 20% bases for which the quality assessment was <20. The clean reads were then aligned to the reference genome using TopHat software, with the alignment having no more than two mismatches or gaps. The gene expression level was calculated by applying the baseMean method. The DEGs were identified by applying the standard of a Student's T-test P-value of <0.05 along with a gene expression level FPKM value of greater than 1.0. The statistics were analysed using the appropriate Microsoft Excel statistical functions.

To understand the functions of the DGEs, GO functional enrichment and Kyoto Encyclopedia of Genes and Genomes (KEGG) pathway analysis were performed using the online server hosting the Princeton GO term finder, which provides functional annotation of biological processes (http://go.princeton.edu/cgi-bin/GOTermFinder) and (http://www.genome.jp/).

4.12. Steps of chemicals intervention

Rapamycin (1 μg/ml) or LY294002 (25 μM) has been added in culture medium to promote or inhibit the autophagy pathway. As shown in SFig.10, the chemicals were added on 3–7 day for 7 days group, or 10–14day for 14days group. DMSO has been used as control.

4.13. Statistical analysis

All data are expressed as mean ± standard deviation (SD). One-way ANOVA was used for multiple comparisons (Duncan's multiple range test) using SPSS ver.13.0 software. P values < 0.05 were considered to be statistically significant.

Credit author statement

Liumin He, Conceptualization, Methodology, Software, Supervision, Zhongqing Sun, Conceptualization, Methodology, Software, Data curation, Writing – original draft, Validation, Jianshuang Li, Conceptualization, Methodology, Software, Validation, Rong Zhu, Conceptualization, Methodology, Software, Data curation, Writing – original draft, Validation, Ben Niu, Software, Validation, Tam Ka Long, Conceptualization, Methodology, Software, Qiao Xiao, Visualization, Investigation, Jun Li, Visualization, Investigation, Wenjun Wang, Visualization, Investigation, Chi Ying Tsui, Visualization, Investigation, Writing-Reviewing and Editing, Vincent Wing Hong Lee, Visualization, Investigation, Writing-Reviewing and Editing, Kwok-Fai So, Writing-Reviewing and Editing, Ying Xu, Writing-Reviewing and Editing, Seeram Ramakrishna, Writing-Reviewing and Editing, Qinghua Zhou, Supervision, Kin Chiu, Supervision, Writing-Reviewing and Editing

Declaration of competing interest

The authors declare that they have no known competing financial interests or personal relationships that could have appeared to influence the work reported in this paper.

Acknowledgements

This work was supported by the National Natural Science Foundation of China (31870964, 32071354), Guangdong province special support plan for high-level talent: Outstanding young scholar in science and technology innovation (2016TQ03R582), National Program on Key Basic Research Project (973 Program, 2014CB542205), the Major Science and Technology Projects of Guangdong Province (2015B020225005), the funds of Leading Talents of Guangdong Province (87014002), the Fundamental Research Funds for the Central Universities to Jinan University (11617439, 89017036, 21617439), and support from KB Woo foundation, the National Natural Science Foundation of China (81800833 and 81802189), the 111 Project (B16021), and the National Key R&D Program of China (2018YFC2002000). All the electrical stimulation devices in this study are provided by Neurotech (Hong Kong) Limited.

Appendix A. Supplementary data

Supplementary data to this article can be found online at https://doi.org/10.1016/j.biomaterials.2020.120585.

References

[1] G.L. Zhang, Z.H. Zhu, Y.Z. Wang, Neural stem cell transplantation therapy for brain ischemic stroke: review and perspectives, World J. Stem Cell. 11 (10) (2019) 817–830.

[2] P. Lu, Y. Wang, L. Graham, K. McHale, M. Gao, D. Wu, J. Brock, A. Blesch, E. S. Rosenzweig, L.A. Havton, B. Zheng, J.M. Conner, M. Marsala, M.H. Tuszynski, Long-distance growth and connectivity of neural stem cells after severe spinal cord injury, Cell 150 (6) (2012) 1264–1273.

[3] E.S. Rosenzweig, J.H. Brock, P. Lu, H. Kumamaru, E.A. Salegio, K. Kadoya, J. L. Weber, J.J. Liang, R. Moseanko, S. Hawbecker, J.R. Huie, L.A. Havton, Y.S. Nout-Lomas, A.R. Ferguson, M.S. Beattie, J.C. Bresnahan, M.H. Tuszynski, Restorative effects of human neural stem cell grafts on the primate spinal cord, Nat. Med. 24 (4) (2018) 484–490.

[4] L.Y. Liao, B.W. Lau, D.I. Sanchez-Vidana, Q. Gao, Exogenous neural stem cell transplantation for cerebral ischemia, Neural Regen Res 14 (7) (2019) 1129–1137.

[5] L.M. McGinley, O.N. Kashlan, E.S. Bruno, K.S. Chen, J.M. Hayes, S.R. Kashlan, J. Raykin, K. Johe, G.G. Murphy, E.L. Feldman, Human neural stem cell transplantation improves cognition in a murine model of Alzheimer's disease, Sci. Rep. 8 (1) (2018) 14776.

[6] Y. Huang, Y. Li, J. Chen, H. Zhou, S. Tan, Electrical stimulation elicits neural stem cells activation: new perspectives in CNS repair, Front. Hum. Neurosci. 9 (2015) 586.

[7] T. Cho, J.K. Ryu, C. Taghibiglou, Y. Ge, A.W. Chan, L. Liu, J. Lu, J.G. McLarnon, Y. T. Wang, Long-term potentiation promotes proliferation/survival and neuronal differentiation of neural stem/progenitor cells, PloS One 8 (10) (2013), e76860.

[8] X. Li, S. Liu, Y. Zhao, J. Li, W. Ding, S. Han, B. Chen, Z. Xiao, J. Dai, Training neural stem cells on functional collagen scaffolds for severe spinal cord injury repair, Adv. Funct. Mater. 26 (32) (2016) 5835–5847.

[9] C.D. McCaig, A.M. Rajnicek, B. Song, M. Zhao, Controlling cell behavior electrically: current views and future potential, Physiol. Rev. 85 (3) (2005) 943–978.

[10] M.A. Matos, M.T. Cicerone, Alternating current electric field effects on neural stem cell viability and differentiation, Biotechnol. Prog. 26 (3) (2010) 664–670.

[11] H. Zhao, A. Steiger, M. Nohner, H. Ye, Specific intensity direct current (DC) electric field improves neural stem cell migration and enhances differentiation towards betaIII-tubulin+ neurons, PloS One 10 (6) (2015), e0129625.

[12] J.F. Feng, J. Liu, L. Zhang, J.Y. Jiang, M. Russell, B.G. Lyeth, J.A. Nolta, M. Zhao, Electrical guidance of human stem cells in the rat brain, Stem Cell Reports 9 (1) (2017) 177–189.

[13] D. Becker, D.S. Gary, E.S. Rosenzweig, W.M. Grill, J.W. McDonald, Functional electrical stimulation helps replenish progenitor cells in the injured spinal cord of adult rats, Exp. Neurol. 222 (2) (2010) 211–218.

[14] J. Du, G. Zhen, H. Chen, S. Zhang, L. Qing, X. Yang, G. Lee, H.Q. Mao, X. Jia, Optimal electrical stimulation boosts stem cell therapy in nerve regeneration, Biomaterials 181 (2018) 347–359.

[15] P.M. George, T.M. Bliss, T. Hua, A. Lee, B. Oh, A. Levinson, S. Mehta, G. Sun, G. K. Steinberg, Electrical preconditioning of stem cells with a conductive polymer scaffold enhances stroke recovery, Biomaterials 142 (2017) 31–40.

[16] X. Li, F. Guo, Q. Zhang, T. Huo, L. Liu, H. Wei, L. Xiong, Q. Wang, Electroacupuncture decreases cognitive impairment and promotes neurogenesis in the APP/PS1 transgenic mice, BMC Compl. Alternative Med. 14 (2014) 37.

[17] T. Fu, L. Jiang, Y. Peng, Z. Li, S. Liu, J. Lu, F. Zhang, J. Zhang, Electrical Muscle Stimulation Accelerates Functional Recovery after Nerve Injury, Neuroscience, 2019.

[18] R.T. Mankowski, S. Ahmed, T. Beaver, M. Dirain, C. Han, P. Hess, T. Martin, B. K. Smith, S. Someya, C. Leeuwenburgh, A.D. Martin, Intraoperative hemidiaphragm electrical stimulation reduces oxidative stress and upregulates autophagy in surgery patients undergoing mechanical ventilation: exploratory study, J. Transl. Med. 14 (1) (2016) 305.

[19] A. Sotthibundhu, W. Promjuntuek, M. Liu, S. Shen, P. Noisa, Roles of autophagy in controlling stem cell identity: a perspective of self-renewal and differentiation, Cell Tissue Res. 374 (2) (2018) 205–216.

[20] L. Casares-Crespo, I. Calatayud-Baselga, L. Garcia-Corzo, H. Mira, On the role of basal autophagy in adult neural stem cells and neurogenesis, Front. Cell. Neurosci. 12 (2018) 339.

[21] J. Dhaliwal, L. Trinkle-Mulcahy, D.C. Lagace, Autophagy and adult neurogenesis: discoveries made half a century ago yet in their infancy of being connected, Brain Plast. 3 (1) (2017) 99–110.

[22] M. Yazdankhah, S. Farioli-Vecchioli, A.B. Tonchev, A. Stoykova, F. Cecconi, The autophagy regulators Ambra1 and Beclin 1 are required for adult neurogenesis in the brain subventricular zone, Cell Death Dis. 5 (2014) e1403.

[23] P. Vazquez, A.I. Arroba, F. Cecconi, E.J. de la Rosa, P. Boya, F. de Pablo, Atg5 and Ambra1 differentially modulate neurogenesis in neural stem cells, Autophagy 8 (2) (2012) 187–199.

[24] H. Shao, P. Zhao, L. Su, L. Tian, Y. Zhang, Y. Sun, S. Yue, W. Xue, S. Ramakrishna, L. He, Fabrication of carbon nanotube nanocomposites via layer-by-layer assembly and evaluation in biomedical application, Nanomedicine 11 (23) (2016) 3087–3101.

[25] X. Sun, H. Shao, K. Xiang, Y. Yan, X. Yu, D. Li, W. Wu, L. Zhou, K.-F. So, Y. Ren, Poly (dopamine)-modified carbon nanotube multilayered film and its effects on macrophages, Carbon 113 (2017) 176–191.

[26] L. He, P. Zhao, Q. Han, X. Wang, X. Cai, Y. Shi, L. Zhou, Y. Zhang, W. Xue, Surface modification of poly-l-lactic acid fibrous scaffolds by a molecular-designed multi-walled carbon nanotube multilayer for enhancing cell interactions, Carbon 56 (2013) 224–234.

[27] Tam Kam Long, Design and Implementation of Biomedical Electrical Etimulation Devises, Hong Kong University of Science and Technology Thesis, 2018.

[28] O.F. Omotade, S.L. Pollitt, J.Q. Zheng, Actin-based growth cone motility and guidance, Mol. Cell. Neurosci. 84 (2017) 4–10.

[29] C. Zuccato, E. Cattaneo, Brain-derived neurotrophic factor in neurodegenerative diseases, Nat. Rev. Neurol. 5 (6) (2009) 311–322.

[30] S. Estes, L. Artinian, V. Rehder, Modulation of growth cone filopodial length by carbon monoxide, Dev Neurobiol 77 (6) (2017) 677–690.

[31] Z. Guo, L. Zhang, Z. Wu, Y. Chen, F. Wang, G. Chen, In vivo direct reprogramming of reactive glial cells into functional neurons after brain injury and in an Alzheimer's disease model, Cell Stem Cell 14 (2) (2014) 188–202.

[32] H.J. Song, C.F. Stevens, F.H. Gage, Neural stem cells from adult hippocampus develop essential properties of functional CNS neurons, Nat. Neurosci. 5 (5) (2002) 438–445.

[33] C. Grienberger, A. Konnerth, Imaging calcium in neurons, Neuron 73 (5) (2012) 862–885.

[34] N.W. Kam, E. Jan, N.A. Kotov, Electrical stimulation of neural stem cells mediated by humanized carbon nanotube composite made with extracellular matrix protein, Nano Lett. 9 (1) (2009) 273–278.

[35] H. Shao, T. Li, R. Zhu, X. Xu, J. Yu, S. Chen, L. Song, S. Ramakrishna, Z. Lei, Y. Ruan, L. He, Carbon nanotube multilayered nanocomposites as multifunctional substrates for actuating neuronal differentiation and functions of neural stem cells, Biomaterials 175 (2018) 93–109.

[36] G. Cellot, E. Cilia, S. Cipollone, V. Rancic, A. Sucapane, S. Giordani, L. Gambazzi, H. Markram, M. Grandolfo, D. Scaini, F. Gelain, L. Casalis, M. Prato, M. Giugliano, L. Ballerini, Carbon nanotubes might improve neuronal performance by favouring electrical shortcuts, Nat. Nanotechnol. 4 (2) (2009) 126–133.

[37] J. Kaur, J. Debnath, Autophagy at the crossroads of catabolism and anabolism, Nat. Rev. Mol. Cell Biol. 16 (8) (2015) 461–472.

[38] M. Ogata, S. Hino, A. Saito, K. Morikawa, S. Kondo, S. Kanemoto, T. Murakami, M. Taniguchi, I. Tanii, K. Yoshinaga, S. Shiosaka, J.A. Hammarback, F. Urano, K. Imaizumi, Autophagy is activated for cell survival after endoplasmic reticulum stress, Mol. Cell Biol. 26 (24) (2006) 9220–9231.

[39] C. Kraft, M. Peter, K. Hofmann, Selective autophagy: ubiquitin-mediated recognition and beyond, Nat. Cell Biol. 12 (9) (2010) 836–841.

[40] G.Y. Liu, D.M. Sabatini, mTOR at the nexus of nutrition, growth, ageing and disease, Nat. Rev. Mol. Cell Biol. 21 (4) (2020) 183–203.

[41] V. Nikoletopoulou, K. Sidiropoulou, E. Kallergi, Y. Dalezios, N. Tavernarakis, Modulation of autophagy by BDNF underlies synaptic plasticity, Cell Metabol. 26 (1) (2017) 230–242 e5.

[42] M.L. Florez-McClure, D.A. Linseman, C.T. Chu, P.A. Barker, R.J. Bouchard, S.S. Le, T.A. Laessig, K.A. Heidenreich, The p75 neurotrophin receptor can induce autophagy and death of cerebellar Purkinje neurons, J. Neurosci. 24 (19) (2004) 4498–4509.

[43] X. Chen, Y. He, F. Lu, Autophagy in stem cell Biology: a perspective on stem cell self-renewal and differentiation, Stem Cell. Int. 2018 (2018) 9131397.

[44] A.L. Morgado, J.M. Xavier, P.A. Dionisio, M.F. Ribeiro, R.B. Dias, A.M. Sebastiao, S. Sola, C.M. Rodrigues, MicroRNA-34a modulates neural stem cell differentiation by regulating expression of synaptic and autophagic proteins, Mol. Neurobiol. 51 (3) (2015) 1168–1183.

[45] Z. Chen, L. Yang, Y. Liu, A. Tang, X. Li, J. Zhang, Z. Yang, LY294002 and Rapamycin promote coxsackievirus-induced cytopathic effect and apoptosis via inhibition of PI3K/AKT/mTOR signaling pathway, Mol. Cell. Biochem. 385 (1–2) (2014) 169–177.

[46] J. Liu, W. Liu, H. Yang, Balancing apoptosis and autophagy for Parkinson's disease therapy: targeting BCL-2, ACS Chem. Neurosci. 10 (2) (2019) 792–802.

[47] Y.J. Huang, H.C. Wu, N.H. Tai, T.W. Wang, Carbon nanotube rope with electrical stimulation promotes the differentiation and maturity of neural stem cells, Small 8 (18) (2012) 2869–2877.

[48] M.K. Gheith, T.C. Pappas, A.V. Liopo, V.A. Sinani, B.S. Shim, M. Motamedi, J. P. Wicksted, N.A. Kotov, Stimulation of neural cells by lateral currents in conductive layer-by-layer films of single-walled carbon nanotubes, Adv. Mater. 18 (22) (2006) 2975–2979.

[49] L. Jin, B. Hu, Z. Li, J. Li, Y. Gao, Z. Wang, J. Hao, Synergistic effects of electrical stimulation and aligned nanofibrous microenvironment on growth behavior of mesenchymal stem cells, ACS Appl. Mater. Interfaces 10 (22) (2018) 18543–18550.

[50] F. Pires, Q. Ferreira, C.A. Rodrigues, J. Morgado, F.C. Ferreira, Neural stem cell differentiation by electrical stimulation using a cross-linked PEDOT substrate: expanding the use of biocompatible conjugated conductive polymers for neural tissue engineering, Biochim. Biophys. Acta 1850 (6) (2015) 1158–1168.

[51] R. Zhu, Z. Sun, C. Li, S. Ramakrishna, K. Chiu, L. He, Electrical stimulation affects neural stem cell fate and function in vitro, Exp. Neurol. 319 (2019) 112963.

[52] Y. Xi, J.S. Dhaliwal, M. Ceizar, M. Vaculik, K.L. Kumar, D.C. Lagace, Knockout of Atg5 delays the maturation and reduces the survival of adult-generated neurons in the hippocampus, Cell Death Dis. 7 (2016) e2127.

[53] C. Wang, C.C. Liang, Z.C. Bian, Y. Zhu, J.L. Guan, FIP200 is required for maintenance and differentiation of postnatal neural stem cells, Nat. Neurosci. 16 (5) (2013) 532–542.

[54] J.O. Pyo, S.M. Yoo, H.H. Ahn, J. Nah, S.H. Hong, T.I. Kam, S. Jung, Y.K. Jung, Overexpression of Atg5 in mice activates autophagy and extends lifespan, Nat. Commun. 4 (2013) 2300.
[55] O.J. Lieberman, A.F. McGuirt, G. Tang, D. Sulzer, Roles for neuronal and glial autophagy in synaptic pruning during development, Neurobiol. Dis. 122 (2019) 49–63.
[56] G. Tang, K. Gudsnuk, S.H. Kuo, M.L. Cotrina, G. Rosoklija, A. Sosunov, M. S. Sonders, E. Kanter, C. Castagna, A. Yamamoto, Z. Yue, O. Arancio, B.S. Peterson, F. Champagne, A.J. Dwork, J. Goldman, D. Sulzer, Loss of mTOR-dependent macroautophagy causes autistic-like synaptic pruning deficits, Neuron 83 (5) (2014) 1131–1143.
[57] R.C. Paolicelli, G. Bolasco, F. Pagani, L. Maggi, M. Scianni, P. Panzanelli, M. Giustetto, T.A. Ferreira, E. Guiducci, L. Dumas, D. Ragozzino, C.T. Gross, Synaptic pruning by microglia is necessary for normal brain development, Science 333 (6048) (2011) 1456–1458.
[58] H.J. Kim, M.H. Cho, W.H. Shim, J.K. Kim, E.Y. Jeon, D.H. Kim, S.Y. Yoon, Deficient autophagy in microglia impairs synaptic pruning and causes social behavioral defects, Mol. Psychiatr. 22 (11) (2017) 1576–1584.
[59] D.P. Schafer, E.K. Lehrman, A.G. Kautzman, R. Koyama, A.R. Mardinly, R. Yamasaki, R.M. Ransohoff, M.E. Greenberg, B.A. Barres, B. Stevens, Microglia sculpt postnatal neural circuits in an activity and complement-dependent manner, Neuron 74 (4) (2012) 691–705.
[60] C. Piochon, M. Kano, C. Hansel, LTD-like molecular pathways in developmental synaptic pruning, Nat. Neurosci. 19 (10) (2016) 1299–1310.
[61] X. Luo, Y. Yu, Z. Xiang, H. Wu, S. Ramakrishna, Y. Wang, K.F. So, Z. Zhang, Y. Xu, Tetramethylpyrazine nitrone protects retinal ganglion cells against N-methyl-d-aspartate-induced excitotoxicity, J. Neurochem. 141 (3) (2017) 373–386.